AD-A150 885 PRESSURE DISTRIBUTION ON PROPELLER BLADE SURFACE USING NUMERICAL LIFTING..(U) DAVID W TAYLOR NAVAL SHIP RESEARCH AND DEVELOPMENT CENTER BET.. K H KIM ET AL. 1/1

UNCLASSIFIED JAN 85 DTNSRDC-84/072 F/G 20/4 NL

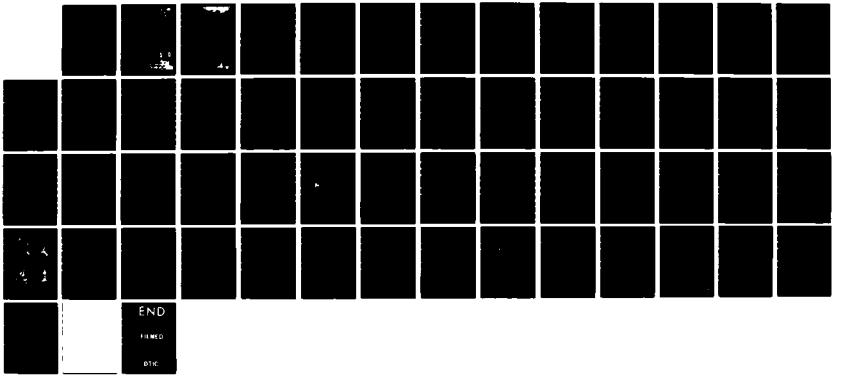

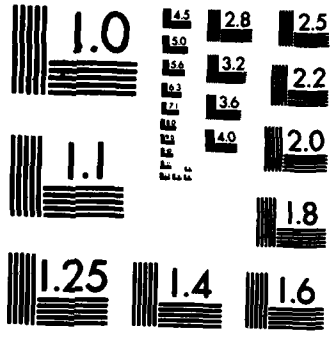

MICROCOPY RESOLUTION TEST CHART
NATIONAL BUREAU OF STANDARDS-1963-A

DAVID W. TAYLOR NAVAL SHIP RESEARCH AND DEVELOPMENT CENTER

Bethesda, Maryland 20084-5000

PRESSURE DISTRIBUTION ON PROPELLER BLADE SURFACE USING NUMERICAL LIFTING SURFACE THEORY

by

Ki-Han Kim
Sukeyuki Kobayashi

APPROVED FOR PUBLIC RELEASE: DISTRIBUTION UNLIMITED

Presented at Propellers 1984 Symposium
Virginia Beach, Va.
15-16 May 1984

SHIP PERFORMANCE DEPARTMENT
RESEARCH AND DEVELOPMENT REPORT

January 1985

PRESSURE DISTRIBUTION ON PROPELLER BLADE SURFACE USING NUMERICAL LIFTING SURFACE THEORY

MAJOR DTNSRDC ORGANIZATION

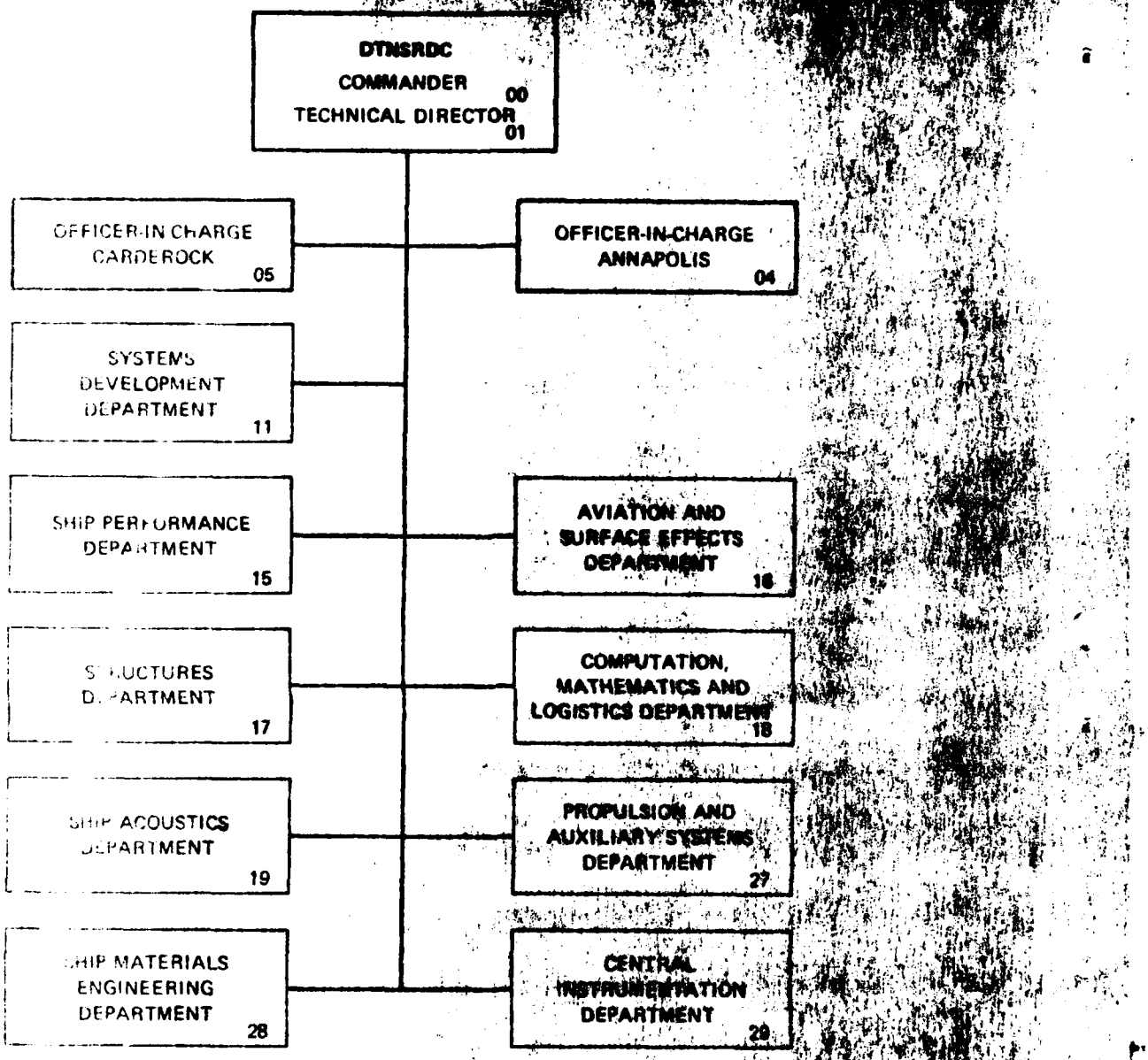

UNCLASSIFIED

SECURITY CLASSIFICATION OF THIS PAGE (When Data Entered)

REPORT DOCUMENTATION PAGE	READ INSTRUCTIONS BEFORE COMPLETING FORM
1. REPORT NUMBER DTNSRDC-84/072	2. GOVT ACCESSION NO. AD-A150885	3. RECIPIENT'S CATALOG NUMBER
4. TITLE (and Subtitle) PRESSURE DISTRIBUTION ON PROPELLER BLADE SURFACE USING NUMERICAL LIFTING SURFACE THEORY	5. TYPE OF REPORT & PERIOD COVERED Final 6. PERFORMING ORG. REPORT NUMBER
7. AUTHOR(s) Ki-Han Kim Sukeyuki Kobayashi	8. CONTRACT OR GRANT NUMBER(s)
9. PERFORMING ORGANIZATION NAME AND ADDRESS David W. Taylor Naval Ship Research and Development Center Bethesda, Maryland 20084-5000	10. PROGRAM ELEMENT, PROJECT, TASK AREA & WORK UNIT NUMBERS
11. CONTROLLING OFFICE NAME AND ADDRESS David W. Taylor Naval Ship Research and Development Center Bethesda, Maryland 20084-5000	12. REPORT DATE January 1985 13. NUMBER OF PAGES 54
14. MONITORING AGENCY NAME & ADDRESS(if different from Controlling Office)	15. SECURITY CLASS. (of this report) UNCLASSIFIED 15a. DECLASSIFICATION/DOWNGRADING SCHEDULE

16. DISTRIBUTION STATEMENT (of this Report)

APPROVED FOR PUBLIC RELEASE: DISTRIBUTION UNLIMITED

17. DISTRIBUTION STATEMENT (of the abstract entered in Block 20, if different from Report)

18. SUPPLEMENTARY NOTES

Presented at Propellers 1984 Symposium, Virginia Beach, Virginia, 15-16 May 1984

19. KEY WORDS (Continue on reverse side if necessary and identify by block number)

Propeller
Blade Pressure
Lifting Surface Theory
Discrete Vortex/Source Method

20. ABSTRACT (Continue on reverse side if necessary and identify by block number)

A procedure and numerical results are presented for the prediction of the steady pressure distribution on a rotating propeller blade surface based on lifting surface theory. A computer code, named the Propeller Steady Pressure (PSP) program, has been developed by extending the existing propeller analysis program, PSF, based on vortex/source lattice techniques, developed at the Massachusetts Institute of Technology. Predictions by

(Continued on reverse side)

DD FORM 1 JAN 73 1473 EDITION OF 1 NOV 65 IS OBSOLETE

S/N 0102-LF-014-6601

UNCLASSIFIED

SECURITY CLASSIFICATION OF THIS PAGE (When Data Entered)

(Block 20 continued)

PSP are compared with selected experimental values that are believed to be accurately and reliably measured. Comparisons are also made between PSP predictions and other theoretical predictions. The predictions by PSP are generally in good agreement with experimental values and with other prediction methods except for the tip region where current procedures may not be accurate enough to represent the actual flow.

Marine propellers ⇒ to pl

Accession For	
NTIS GRA&I	☒
DTIC TAB	☐
Unannounced	☐
Justification	
By	
Distribution/	
Availability Codes	
Dist	Avail and/or Special
A-1	

TABLE OF CONTENTS

	Page
LIST OF FIGURES	iii
TABLE	iv
NOTATION	v
ABSTRACT	1
INTRODUCTION	1
OVERVIEW OF PSP	2
MODIFICATION TO PSF	4
RESULTS AND DISCUSSIONS	8
TWO-DIMENSIONAL AIRFOIL SECTIONS	8
IHI MODEL PROPELLER MP 282	8
DTNSRDC PROPELLER 4718	10
NSMB MODEL PROPELLER	11
COMPARISON WITH OTHER PROCEDURES	11
SUMMARY AND CONCLUSIONS	12
RECOMMENDATIONS	13
ACKNOWLEDGMENT	13
REFERENCES	15
APPENDIX - PRESSURE IN A MOVING FRAME OF REFERENCE	17

LIST OF FIGURES

1 - Fixed and Rotating Coordinate Systems for a Right-Hand-Rotation Propeller	21
2 - Discretization of Blade Singularities	22
3 - Horseshoe Vortices on Blade and in Wake	23
4 - Trailing Wake Geometry after Wake Alignment	24
5 - Discrete Singularity Distribution for Two-Dimensional Airfoil Section	25

6 - Schematic Representation of the Effect of Chordwise Vortices on the i^{th} Pressure Point 26

7 - Pressure Distribution on Flat Plate at α = 4 Degrees 27

8 - Pressure Distribution on NACA 0012 Section at α = 0 Degrees 28

9 - Pressure Distribution on NACA 4412 Section at α = 6.4 Degrees 29

10 - Open-Water Performance of IHI Model Propeller MP 282 30

11 - Pressure Distribution on IHI Model Propeller MP 282 at J = 1.054 31

12 - Pressure Distribution on IHI Model Propeller MP 282 at J = 1.163 32

13 - Surface Flow Patterns by Oil-Film Test on IHI Model Propeller MP 282 33

14 - Pressure Distribution on DTNSRDC Propeller 4718 at J = 0.75 34

15 - Pressure Distribution on Suction Side of DTNSRDC Propeller 4718 at r/R = 0.5: Comparison of Prediction and Two Sets of Experiments 35

16 - Open-Water Performance of NSMB Model Propeller 36

17 - Pressure Distribution on NSMB Propeller at J = 0.4 37

18 - Pressure Distribution on NSMB Propeller at J = 0.6 39

19 - Pressure Distribution on DTNSRDC Propeller 4118 at J = 0.833: Comparison with ITTC Propeller Committee Survey 41

20 - Pressure Distribution on DTNSRDC Propeller 4498 at J = 0.888 42

Table 1 - Propeller Geometric Characteristics 43

NOTATION

c	Blade-section chord length
$C_p = (p-p_\infty)/(\rho V_R^2/2)$	Pressure coefficient
D	Propeller Diameter
f	Meanline shape function
g	Gravitational acceleration
$(\underline{i},\underline{e}_r,\underline{e}_\theta)$	Unit base vectors in a cylindrical polar reference system
$(\underline{i},\underline{j},\underline{k})$	Unit base vectors in a Cartesian reference frame
i_T	Total rake: axial displacement of blade-section midchord point from y-z plane
$J = V/nD$	Advance coefficient
$K_Q = Q/(\rho n^2 D^5)$	Torque coefficient
$K_T = T/(\rho n^2 D^4)$	Thrust coefficient
n	Propeller rotational speed, revolutions per unit time
P	Pitch of blade section
p	Pressure
p_∞	Ambient pressure
Q	Torque absorbed by blades, or strength of discrete line source per unit length
q	Distributed source strength
R	Propeller radius
r	Radial coordinate
$\underline{r}$	Position vector of field point
T	Thrust produced by blades
t	Thickness shape function

$\underline{V}$	Total velocity vector
V_R	Reference speed
(x,y,z)	Cartesian coordinates fixed on propeller
(x_o,y_o,z_o)	Cartesian coordinates in inertial reference frame
x_c	Fraction of chord, measured from leading edge
x_R	Fraction of radius, measured from axis of rotation
Z	Number of blades
α	Angle of attack
Γ	Strength of discrete bound vortex for two-dimensional airfoil
$\underline{\Gamma}_c$	Chordwise discrete vortex on the blade surface
$\underline{\Gamma}_s$	Spanwise discrete vortex on the blade surface
$\gamma = \gamma_c + \gamma_s$	Total distributed vortex on the blade surface
γ_c	Chordwise distributed vortex on the blade surface
γ_s	Spanwise distributed vortex on the blade surface
$\theta = \tan^{-1}(z/y)$	Angular coordinate in propeller-fixed coordinates
$\theta_o = \tan^{-1}(z_o/y_o)$	Angular coordinate in inertial reference frame
θ_s	Skew angle; circumferential displacement of blade-section midchord point from z=0 plane
ρ	Fluid density
ϕ	Pitch angle of blade section nose-tail line; measured on cylinder of radius r
$\Omega = 2\pi n$	Propeller rotational speed; radians per unit time
$\underline{\omega}$	Vorticity vector in flow field

ABSTRACT

A procedure and numerical results are presented for the prediction of the steady pressure distribution on a rotating propeller blade surface based on lifting surface theory. A computer code, named the Propeller Steady Pressure (PSP) program, has been developed by extending the existing propeller analysis program, PSF, based on vortex/source lattice techniques, developed at the Massachusetts Institute of Technology. Predictions by PSP are compared with selected experimental values that are believed to be accurately and reliably measured. Comparisons are also made between PSP predictions and other theoretical predictions. The predictions by PSP are generally in good agreement with experimental values and with other prediction methods except for the tip region where current procedures may not be accurate enough to represent the actual flow.

INTRODUCTION

Knowledge of the pressure distribution on the propeller blade surface is essential to understanding cavitation phenomena, boundary layer characteristics and stress on blades. Measuring the pressure distribution on a rotating blade is extremely difficult and time-consuming, and even then the reliability and repeatability of the experimental data are often questionable. Nevertheless, a number of experimental results of reasonable reliability are available, such as the ones obtained by Mavludoff,[1*] Kato,[2] Yamasaki,[3] Takei et al.,[4] Jessup,[5] and Versmissen and Van Gent.[6]

The ability to predict the blade pressure distribution reliably and accurately is also highly desirable. Many institutions throughout the world have their own prediction methods; most of them are based on lifting-surface methods such as those of Okamura,[7] Kuiper,[8] Brockett,[9] and Tsakonas et al.[10] and a two-dimensional procedure with some empirical corrections for three-dimensional effects by Bahgat.[11]

In this report, a procedure is presented to predict the pressure distribution on the propeller blade surface operating in steady flow based on the discrete vortex/source lattice method developed by Greeley and Kerwin.[12] The discrete vortex lattice method has been used in the field of aerodynamics as early as 1943

---

*A complete listing of references is given on page 15.

by Faulkner[13] for the calculation of aerodynamic forces on an arbitrary wing shape. The accuracy of this simple method has been found very satisfactory[14] and in two-dimensional flow "remarkable".[15] The primary advantage in using the discrete vortex/source lattice method is the ease and the flexibility to model the complex geometries of the propeller blades and their trailing vortex wake. With the advent of large computers, panel methods are widely used for the design and analysis of three-dimensional aerodynamic configurations both as the simple vortex/source lattice approximation and as more complex local elements.

In the area of marine hydrodynamics, Kerwin and Lee[16] developed a discrete vortex/source method and corresponding computer code, PUF2, for the prediction of steady and unsteady performance of subcavitating propellers. Kobayashi[17] and Kim[18] developed a procedure to compute the pressure distribution based on the method developed by Kerwin and Lee.[16] More recently, Greeley and Kerwin[12] developed design and analysis procedures and corresponding computer codes, PBD-10 for design and PSF for analysis, for propellers operating in steady flow. Greeley and Kerwin[12] made improvements to the steady part of the procedure developed by Kerwin and Lee[16] in two major areas; one is the improved semi-empirical description of the trailing vortex sheet and the other is the capability to model the flow over the outer portion of the blade more accurately. In the present work, only the "global" part of the procedure developed by Greeley and Kerwin[12] has been investigated for the pressure distribution. The more accurate local flow model near the tip is yet to be examined.

A computer code, named the Propeller Steady Pressure (PSP) program, has been developed by extending the propeller analysis program, PSF, presented by Greeley[19] and Greeley and Kerwin.[12] This report describes the computer code and presents some comparisons of the predictions made by PSP with experimental measurements and predictions by other theories.

OVERVIEW OF PSP

The Propeller Steady Pressure (PSP) code is basically the same as the Propeller Steady Flow (PSF) analysis program developed by Greeley and Kerwin,[12] except for the additional capability in PSP of calculating the pressure distribution on the blade surface. The PSF code assumes that the propeller operates in an axisymmetric onset flow consisting of axial, radial, and tangential components. The presence of the propeller hub and any other boundaries to the flow is ignored. The blade

boundary layers are assumed to be thin, so that the flow can be treated as inviscid, except for the calculation of frictional drag.

The nonrotating coordinate system, (x_o,y_o,z_o), and rotating coordinate system, (x,y,z), fixed to the blades are shown in Figure 1. The x-axis of the fixed and rotating system are coincident, as are the (y,z) and (y_o,z_o) planes. The definition of the angular coordinates in the fixed system, θ_o, and in the rotating system, θ, are also defined in Figure 1. The propeller rotates at a constant angular velocity, $\underline{\Omega} = -\Omega\underline{i}$. A field point, P, in the fluid with angular coordinate, θ, in the rotating frame has an angular coordinate

$$\theta_o = \theta - \Omega t \tag{1}$$

in the fixed frame for a right-handed propeller shown in Figure 1.

The blade geometry is defined relative to a midchord line, which is parametrically defined by the radial distribution of skew, $\theta_s(r)$, and total rake, $i_T(r)$. The pitch angle, $\phi(r)$, and chord length, $c(r)$, define the angle and extent of the sectional nose-tail line along the pitch helix on the surface of a cylinder of radius r. The meanline offset, $f(r,x_c)$, and thickness distribution, $t(r,x_c)$, describe the section characteristics of the blade as a function of radius, r, and nondimensional arc length, x_c, along the nose-tail line. The meanline, f, is measured along the cylindrical surface at right angles to the nose-tail line. The thickness, t, is measured perpendicular to the meanline.*

The blades and vortex wake are represented by straight-line vortex and source lattice elements of constant strength, distributed over the meanline surface of the blade (see Figure 2) and the assumed surface of the trailing vortex sheet. The vortices are arranged in the traditional horseshoe configuration (see Figure 3) so as to satisfy Kelvin's conditions automatically, and the strength of each horseshoe vortex is determined by solving a set of simultaneous equations, each satisfying the flow tangency condition at a blade control point. Source strength is determined from the slope of the thickness distribution and resultant onset speed.

* At DTNSRDC, the thickness is conventionally measured perpendicular to the nose-tail line. In linear theory the differences of these two specifications is of higher order.

The position of the shed vortex sheet is determined iteratively by first solving the boundary value problem with an assumed position, and then aligning the wake with the computed total velocity field for a specified radial contraction. The boundary value problem is then re-solved and the procedure is repeated until convergence (see Figure 4). This process of wake alignment is different from the simple wake model in PUF2,[16] where the trailing vortex wake geometry is defined at the outset by several semi-empirically determined geometric parameters.

Once a converged solution is obtained, blade forces are computed by applying the Kutta-Joukowski and Lagally theorems. The Lagally theorem is used to compute the forces on the source elements as a modification for the effect of the thickness (source).[16] This modification is equivalent to subtracting the thickness-induced velocity from the total velocity used to compute the Kutta-Joukowski force on the vortex elements. If the thickness-induced velocity were included in the total velocity, the resulting Kutta-Joukowski force would be larger than experimental values. In PSF, as in PUF2, an empirical suction factor is used to estimate the leading-edge suction force at off-design conditions. The reader is referred to Greeley and Kerwin[12] for details of the computation.

MODIFICATIONS TO PSF

In PSF, the overall blade load is computed by summing up the elementary loads (the jump in pressure across the surface) acting on each line vortex and source element. The elementary load is computed at the midpoint of each spanwise and chordwise singularity on the key blade by assuming the average velocity over the length of a singularity can be approximated by the velocity at its midpoint. This point is called "load point." Since the total velocity is calculated at each load point to compute the load, it is logical to choose the same point as the "pressure point" for pressure calculation. In the present study, pressure is computed at only the pressure points on the spanwise singularities and is interpolated at specified radii.

The velocity calculated at the load point in PSF is a mean velocity that does not include the self-induced velocity due to the singularity segment where the elementary load is calculated. However, when computing the pressure, not the jump in pressure, the velocity jump across the singularity must be included.

Since the vortex/source sheet on the blade surface is represented by "discrete" singularity elements, each discrete element represents a certain area. Therefore, when computing the velocity jump across the vortex sheet, we have to redistribute this concentrated vortex/source over the area.

Consider a two-dimensional airfoil illustrated in Figure 5. The discrete bound vortices/sources are located on the meanline at the quarter chord of each meanline segment to approximate the continuous distribution of the vortex/source along the meanline. Suppose Γ_i is the strength of the bound vortex at the i^{th} segment whose length is Δc_i. Then the distributed vortex strength, γ_i, over this segment can be approximated by:

$$\gamma_i = \frac{\Gamma_i}{\Delta c_i} \tag{2}$$

assuming the vorticity is uniformly distributed over the segment. The velocity jump across the vortex sheet is related to the local vortex strength, γ_i, as follows:

$$(V_t)_i^+ = \frac{\gamma_i}{2} \quad \text{and} \quad (V_t)_i^- = -\frac{\gamma_i}{2} \tag{3}$$

where the plus sign represents the upper surface and the minus sign the lower surface. In this two-dimensional case, the velocity jump is tangent to the surface in the chordwise direction.

Similarly, the distributed source strength, q_i, over the same segment will be:

$$q_i = \frac{Q_i}{\Delta c_i} \tag{4}$$

where Q_i is the strength of the discrete source element. The source sheet induces a jump in normal velocity, that is related to the local source strength, q_i, as follows:

$$(V_n)_i^+ = \frac{q_i}{2} \quad \text{and} \quad (V_n)_i^- = -\frac{q_i}{2} \tag{5}$$

where the plus and minus signs represent the upper and lower surfaces, respectively.

For three-dimensional flow such as that on propeller blades, the direction of velocity jump depends on both the spanwise and chordwise vortices. In this case, both spanwise and chordwise singularities have to be properly accounted for when computing the velocity jump. The following is the algorithm adopted in the present study.

Suppose we want to compute the velocity jump at the i^{th} pressure point on i^{th} spanwise vortex element. The total distributed vortex at this point, $\underline{\gamma}_i$, is the sum of the spanwise and chordwise distributed vortices:

$$\underline{\gamma}_i = (\underline{\gamma}_s)_i + (\underline{\gamma}_c)_i \tag{6}$$

The spanwise distributed vortex, $(\underline{\gamma}_s)_i$, is approximated by:

$$(\underline{\gamma}_s)_i = \frac{(\underline{\Gamma}_s)_i}{\Delta c_i} \tag{7}$$

where Δc_i is the length of the chordwise segment represented by the discrete spanwise vortex, $(\underline{\Gamma}_s)_i$. This is analogous to the two-dimensional distributed bound vortex (see Equation (2)). The chordwise distributed vortex, $(\underline{\gamma}_c)$, is approximated by the vector average of the four adjacent chordwise vortices, $(\underline{\Gamma}_c)_1$, $(\underline{\Gamma}_c)_2$, $(\underline{\Gamma}_c)_3$, and $(\underline{\Gamma}_c)_4$ (see Figure 6):

$$(\underline{\gamma}_c)_i = \frac{1}{4} \sum_{i=1}^{4} \frac{(\underline{\Gamma}_c)_n}{\Delta r_n} \tag{8}$$

where Δr_n is the length of the radial segment represented by each discrete chordwise vortex, $(\underline{\Gamma}_c)_n$. The total distributed vortex, $\underline{\gamma}_i$, is then converted to the velocity jump in the tangential direction by using Equation (3).

The velocity jump due to the source sheet is identical to the two-dimensional case (see Equation (5)) since the boundary condition for thickness effects results in the same relation between source strength and slope of the chordwise thickness distribution with radius as a parameter. These velocity jumps due to vortices and sources are added to the velocity induced by all other singularities to obtain the total velocity induced by the propeller.

The pressure on a propeller blade surface rotating at a constant angular velocity, $\underline{\Omega} = -\Omega\underline{i}$ (see Figure 1), in an axisymmetric onset flow can be expressed as (see Appendix):

$$p = -\frac{1}{2}\rho\{\underline{V}\cdot\underline{V} - (V_x)_A^2 - r^2\Omega^2\} + p_A \tag{9}$$

where $\underline{V}$ = total velocity; $\underline{V} = \underline{V}_w + r\Omega\underline{e}_\theta + \underline{V}_p + \underline{V}_o$

$\underline{V}_w$ = axisymmetric onset flow; $\underline{V}_w = V_x\underline{i} + V_r\underline{e}_r + V_\theta\underline{e}_\theta$

$\underline{V}_p$ = perturbation velocity due to the propeller blades and their wakes

$\underline{V}_o$ = perturbation velocity due to the other sources such as appendages or lifting surfaces

$(\underline{i},\underline{e}_r,\underline{e}_\theta)$ = unit vectors in the axial, radial and tangential directions in the cylindrical coordinate system (x,r,θ) rotating with the propeller

The subscript, A, in Equation (9) indicates a point on the same streamline where the pressure is computed.

If a propeller is operating in a uniform onset flow with only an axial component and with no other sources of disturbance, i.e., the flow condition for all the experimental measurements correlated in this report, the pressure will be:

$$p = -\frac{1}{2}\rho\{\underline{V}\cdot\underline{V} - V_x^2 - r^2\Omega^2\} + p_\infty \tag{10}$$

where $\underline{V} = V_x\underline{i} + r\Omega\underline{e}_\theta + \underline{V}_p$, and p_∞ is the pressure at any point far upstream of a propeller.

We define the pressure coefficient C_p as

$$C_p = \frac{p - p_\infty}{\frac{1}{2}\rho V_R^2} = -\frac{1}{V_R^2}(\underline{V}\cdot\underline{V} - V_x^2 - r^2\Omega^2) \tag{11}$$

where V_R is a reference speed. In PSP, three options are given for V_R; one is the local inflow speed to the blade section, $\sqrt{V_x^2 + (2\pi nr)^2}$, the other two options are the local inflow speed at r = 0.7R and the ship speed.

RESULTS AND DISCUSSIONS

The procedure to calculate the pressure distribution presented in the preceding section has been applied to the following configurations:

1. Two-dimensional airfoil sections; flat plate, NACA 0012 and NACA 4412 sections
2. IHI Propeller MP 282
3. DTNSRDC Propeller 4718
4. NSMB Model Propeller
5. DTNSRDC Propeller 4118
6. DTNSRDC Propeller 4498

The geometric characteristics of these propellers are summarized in Table 1. The predictions by PSP are compared with either experimental measurements or other theoretical predictions.

TWO-DIMENSIONAL AIRFOIL SECTIONS

In order to test the validity of the discrete vortex/source lattice method for pressure computation, a computer program, FOIL2D, was developed for computing the pressure distribution on two-dimensional airfoil sections. FOIL2D has all the ingredients of the discrete vortex/source lattice method except for three-dimensional effects.

Figure 7 shows the comparison of the predicted pressure distribution on a flat plate with an angle of attack $\alpha = 4$ degrees by FOIL2D with the analytical solution in Reference 20. In Figure 8, the pressure distribution is compared for the analytical solution[20] and the FOIL2D predictions on the NACA 0012 section at zero angle of attack. In Figure 9, measured pressure distribution on NACA 4412 section at $\alpha = 6.4$ degrees is compared with predictions by different methods including FOIL2D. Agreements between the predictions by FOIL2D and experiments as well as those between the former and other prediction methods are excellent for two-dimensional shapes.

IHI MODEL PROPELLER MP 282

The open-water performance and the pressure distribution were computed on the Ishikawajima-Harima Heavy Industries (IHI) large model propeller MP 282 operating in uniform flow. The diameter of the propeller is 0.95 m. This propeller has radially varying meanline and thickness distribution. The predictions are

compared with the experimental measurements performed using individual tubes to a hub sensor made at IHI Ship Model Basin.[3,21]

The open-water performance was calculated and compared with experimental results in Figure 10. The predicted K_T values are in excellent agreement with experimental measurements. The predicted K_Q values are about 5 percent greater than the experimental values over the range of advance coefficients.

The pressure distribution on the blade of Propeller MP 282 was calculated for two different J values; J = 1.054 and J = 1.163. The pressure coefficients were calculated on both the suction and the pressure sides at selected radii (r/R = 0.6, 0.7, 0.8, 0.9).

In Figures 11 and 12, the experimental measurements and the predicted C_p are compared at J = 1.054 and J = 1.163, respectively. The experimental measurements were made at a Reynolds number, $R_n = 1.9 \times 10^6$. The calculated pressure coefficients are in good agreement with measurements on the pressure side except near the leading edge, but generally overpredict the suction side pressure. The agreement at the reduced J value is better than that at the increased J value. In general, the predicted values are in satisfactory agreement with the experimental measurements throughout the radius at the two different J values.

In Figure 13, the oil-film test results reconstructed from the photographs in Reference 21 are shown at two Reynolds numbers; 1.1×10^6 and 2.6×10^6. The oil film illustrates the surface streamlines on both sides of the blade. At the reduced R_n condition, the flow patterns on the suction side have significantly reduced shear stress over the forward part of the blade and a clear separation occurs slightly past midchord. On the pressure side, reduced shear regions occur toward the leading edge and some indication of a leading-edge laminar separation bubble occurs at both Reynolds numbers.

No surface flow patterns are presented in Reference 21 for the test R_n of 1.9×10^6. However, judging from the measured pressure coefficients shown in Figures 11 and 12, it is possible that separation occurred near 0.7 fraction of chord on the suction side and at the leading edge on the pressure side in the form of a bubble. Such separation would explain the suction peak on the pressure side near the leading edge and the pressure peak measured at 0.7 radius at 0.7 fraction of chord (measurements were not made at a similar chordwise position at other radii). It is further hypothesized that the suction side separation is a thin

layer with only minor influence on the pressure away from the separation line. Previous data[3] for this propeller indicated that the pressure at the point in question exhibited the same property as a function of Reynolds number.

DTNSRDC PROPELLER 4718

The steady pressure distribution was calculated on the surface of DTNSRDC controllable-pitch Propeller 4718 at the design advance coefficient, J = 0.75. The propeller has three blades with diameter of 2 feet (0.61 meters), EAR of 0.44, and tip skew of 20 degrees. In Figure 14, the predicted pressure coefficients are compared with experimental measurements[5] on the blade surface with the propeller operating in uniform flow at three different radii; r/R = 0.5, 0.7, and 0.9. The pressure was measured by transducers mounted on both sides of the blade surface.

The experimental values were measured at six different R_n values ranging from 2.5×10^6 to 4.63×10^6 at the design J. For this range of R_n, the flow on the surface should be fully turbulent so that the pressure distribution would be nearly independent of R_n. However, the experimental measurements showed substantial variations for different R_n values. The variation is more pronounced on the suction side than on the pressure side. In general, the pressure coefficients increase with increasing R_n values. The measured pressure coefficients shown in Figure 14 represent the average values over the range of R_n. Unpublished flow visualization* of the surface streamlines showed no anomolous flow over the blades.

At r/R = 0.7, the computed values are in reasonable agreement with experimental values. However, the agreement at the other two radii is not as good as that at r/R = 0.7. At r/R = 0.5, the experimental results show some irregular peaks at x_c = 0.12 and 0.5 on both sides. Jessup[5] explained that some of these irregularities in the measured values might be partially attributed to the effect of the relatively large fairwater and hub.

More recently, Jessup* measured blade pressure on the same Propeller 4718 using another technique. In this experiment, Jessup measured the pressure distribution only on the suction side at two radii, r/R = 0.5 and 0.8 at the design J = 0.751. In Figure 15, the two sets of experimental values are compared with PSP

---

*Private communication from S. Jessup, DTNSRDC, Code 1544.

predictions. Although both experimental measurements showed Reynolds number effects, the correlation between PSP predictions and the new experimental values improved substantially.

The larger discrepancy at r/R = 0.9 on the suction side may be due to real flow effects. However, experimental inaccuracy demonstrated at r/R = 0.5, or the coarse modeling for the global solution in the analytic treatment of the flow in that region can also be a possible source of the discrepancy.

NSMB MODEL PROPELLER

The steady pressure distribution was computed on the NSMB model propeller at J = 0.4 and 0.6 to correlate with experimental data.[6] This propeller has simple geometric characteristics; no rake, no skew, and a single section shape over the radius. It was originally designed for bubble cavitation investigation.

The open-water performance was calculated and compared with experimental results in Figure 16. The predicted K_T and K_Q are in excellent agreement with the experimental values for the range of J values except for very reduced ones.

In Figures 17 and 18, the predicted pressure coefficients are compared with experimental measurements obtained at NSMB[6] at J = 0.4 and 0.6, respectively, at five different radii; r/R = 0.4, 0.5, 0.6, 0.7, and 0.8. At r/R = 0.9, only predicted values are plotted since the pressure was not measured at that radius. The pressure was measured by transducers mounted within both sides of the blade surface.

The experimental measurements were made twice within a six-month period in order to assess the repeatability. The two series of experimental results are shown in Figures 17 and 18. The repeatability is generally good. The predicted values on both sides are in good agreement with experimental measurements at both J values.

COMPARISON WITH OTHER PROCEDURES

In 1978, the ITTC Propeller Committee surveyed existing prediction methods for pressure distribution on the propeller blade surface.[22] They compared the predictions made by various methods from sixteen participating institutions throughout the world. The propeller selected for the comparative calculations was DTNSRDC Propeller 4118, a three-bladed research propeller tested thoroughly at DTNSRDC for open-water performance, cavitation, and unsteady forces.

In Figure 19, the predictions by PSP are compared with other predictions represented by the envelope covering all the predicted results at the design advance coefficient, J = 0.833. The predicted values by PSP are within the envelope of the predictions by other methods.

In Figure 20, comparisons are made between predictions by PSP and by a lifting surface method presented by Brockett[9*] for a propeller similar to DTNSRDC Propeller 4498 at J = 0.888. The propeller is warped with 72 degrees warp angle at the tip. The section meanline is similar to the NACA a = 0.8 meanline.

The predictions made by the two different methods are in good agreement at r/R = 0.254, but the discrepancies increase toward the tip region, as it did for the experimental data of Jessup.

SUMMARY AND CONCLUSIONS

The discrete vortex/source lattice lifting surface method has been used for the prediction of steady pressure distribution on a rotating propeller blade surface. A computer code, PSP, has been developed by extending the existing propeller global analysis program, PSF, developed at M.I.T.

For pressure computations on the propeller blades, the velocity jump across the vortex/source sheet must be carefully treated and include the effects of both the spanwise and chordwise vortices. In PSP, the effect of the chordwise vortices at the pressure point, the midpoint of each spanwise vortex, was accounted for by interpolating from the four adjacent chordwise vortices.

Comparisons of the predictions by PSP with experimental measurements and predictions by other methods on selected model propellers generally showed good correlations. The correlations near the tip region, especially for skewed propellers, i.e., Propellers 4718 (20 degrees tip skew) and 4498 (72 degrees tip skew), are not as good as those for the inner region. Possible explanations may be that near the tip region of skewed propellers, viscous effects may be large or that the current numerical modeling in lifting surface representations may not be accurate enough.

---

*The predictions by Brockett shown in Figure 20 are taken from Figure A (linear 3D method) in "Discussions and Authors' Closures" section of Reference 9.

RECOMMENDATIONS

Based on the investigations made in the present work, the following studies are recommended in order to further improve the current prediction method:

1. The improved-accuracy, tip-flow part of the PSF should be used for the prediction of the pressure distribution near the tip region. The tip flow is very complicated and of practical importance, and yet the prediction near the tip region is not as good as that for the inner region. Since the tip flow model contains a finer lattice arrangement than does the global flow model, the tip flow solution is expected to give more accurate results. The modification to the tip flow part for pressure calculations is straightforward.

2. In order to be able to predict viscous phenomena such as suction-side separation or leading-edge laminar bubble separation that is frequently observed in experiments with model propellers, suitable analytical and numerical analysis should be undertaken. Some initial efforts in this area have been undertaken.[12]

3. In order to further assess the validity and limitation of the current procedure, comparative calculations are recommended with other theories for a wide range of propellers and operating conditions.

4. Parametric calculations of propeller characteristics of practical importance such as cavitation inception, boundary layer development, and blade stress should be undertaken.

ACKNOWLEDGMENT

The authors are very grateful to Dr. Terry Brockett of DTNSRDC for many helpful comments and criticisms during the preparation of this report.

REFERENCES

1. Mavludoff, M.A., "Measurement of Pressure on the Blade Surface of a Non-Cavitating Propeller Model," Proceedings, 12th I.T.T.C., Tokyo, Japan (1965).

2. Kato, H., "An Experimental Study on the Pressure Fluctuations on a Propeller Blade in a Wake," Proceedings, Symposium on Hydrodynamics of Ship and Offshore Propulsion Systems, Oslo, Norway (Mar 1977).

3. Yamasaki, T., "On Some Tank Test Results with a Large Model Propeller - 0.95 m in Diameter, Part I," Journal of the Society of Naval Architects of Japan, Vol. 144 (Dec 1978).

4. Takei, Y. et al., "Measurements of Pressures on a Blade of a Propeller Model," Ship Research Institute, Paper No. 55, Tokyo, Japan (1979).

5. Jessup, S.D., "Measurement of the Pressure Distribution on Two Model Propellers," DTNSRDC Report 82/035 (Jul 1982).

6. Versmissen, G.G.P. and W. Van Gent, "Hydrodynamic Pressure Measurements on a Ship Model Propeller," Proceedings, 14th Symposium on Naval Hydrodynamics, National Academy Press, Washington, D.C. (1983).

7. Okamura, N., "Practical Calculating Method of Propeller Characteristics under Viscous Effects," IHI Engineering Review, Vol. 10, No. 2, Tokyo, Japan (Apr 1977).

8. Kuiper, G., "Scale Effects on Propeller Cavitation Inception," Proceedings, 12th Symposium on Naval Hydrodynamics (Jun 1978).

9. Brockett, T.E., "Lifting Surface Hydrodynamics for Design of Rotating Blades," Proceedings, SNAME Propellers '81 Symposium (May 1981).

10. Tsakonas, S. et al., "Blade Pressure Distribution for a Moderately Loaded Propeller," Journal of Ship Research, Vol. 27, No. 1 (Mar 1983).

11. Bahgat, F., "Propeller Blade Pressure Distribution at Part Load," Proceedings, ISSHES-83 International Symposium on Ship Hydrodynamics and Energy Saving, El Pardo, Spain (Sep 1983).

12. Greeley, D.S. and J.E. Kerwin, "Numerical Methods for Propeller Design and Analysis in Steady Flow," Transactions SNAME, Vol. 90 (1982).

13. Faulkner, V.M., "The Calculation of Aerodynamic Loading on Surfaces of Any Shape," British Aeronautical Research Council, R & M 1910 (1943).

14. Faulkner, V.M., "The Scope and Accuracy of Vortex Lattice Theory," British Aeronautical Research Council, R & M 2740 (1949).

15. James, R.M., "On the Remarkable Accuracy of the Vortex Lattice Method," Computer Methods in Applied Mechanics and Engineering, Vol. 1, No. 1 (Jun 1972).

16. Kerwin, J.E. and C.S. Lee, "Prediction of Steady and Unsteady Marine Propeller Performance by Numerical Lifting Surface Theory," Transactions SNAME, Vol. 86 (1978).

17. Kobayashi, S., "Prediction of Pressure Distribution on Propeller Blade Surface Using Numerical Lifting Surface Theory," ORI, Inc. Technical Report No. 2117 (Oct 1982).

18. Kim, K.H., "Correlation of Pressure Distribution on the Blade of ITTC Propeller Committee Model Propeller MP 282," DTNSRDC/SPD-1093/01 (Feb 1984).

19. Greeley, D.S., "Marine Propeller Blade Tip Flows," Massachusetts Institute of Technology, Department of Ocean Engineering Report No. 82-3 (1982).

20. Abbot, I.H. and A.E. Von Doenhoff, "Theory of Wing Sections," Dover Publications, New York (1949).

21. Namimatsu, M., "Experiments for MP 282 Large-Scale Model Propeller," IHI Ship Model Basin Report No. 450-0, Yokohama, Japan (1978).

22. Report of Propeller Committee, Proceedings, 15th International Towing Tank Conference (1978).

23. Batchelor, G.K., "An Introduction to Fluid Dynamics," Cambridge University Press (1967).

APPENDIX

PRESSURE IN A MOVING FRAME OF REFERENCE

In a moving frame of reference, Euler's equation of motion of an inviscid and incompressible fluid can be expressed as follows (see Batchelor[23]):

$$\frac{D\underline{V}}{Dt} = -\frac{1}{\rho}\nabla p + \underline{F} - \left\{\frac{d^2\underline{r}_o}{dt^2} + \frac{d\underline{\Omega}}{dt} \times \underline{r} + 2\underline{\Omega} \times \underline{V} + \underline{\Omega} \times (\underline{\Omega} \times \underline{r})\right\} \tag{12}$$

where $\frac{D}{Dt}$ = material derivative defined by $\frac{D}{Dt} = \frac{\partial}{\partial t} + \underline{V} \cdot \nabla$

$\underline{V}$ = total velocity with respect to the moving reference frame

ρ = fluid density

p = pressure

$\underline{F}$ = body force per unit mass

$\underline{r}_o$ = position vector of the origin of the moving frame

$\underline{\Omega}$ = angular velocity of the moving frame about the origin

$\underline{r}$ = position vector of a field point in the moving frame

The last two terms, $2\underline{\Omega} \times \underline{V}$ and $\underline{\Omega} \times (\underline{\Omega} \times \underline{r})$, are called the Coriolis force and the centrifugal force, respectively.

If we take $\underline{r}_o = 0$ and $\underline{\Omega}$ = constant, Equation (12) becomes:

$$\frac{\partial \underline{V}}{\partial t} + (\underline{V} \cdot \nabla)\underline{V} = -\frac{1}{\rho}\nabla p + \underline{F} - 2\underline{\Omega} \times \underline{V} - \underline{\Omega} \times (\underline{\Omega} \times \underline{r}) \tag{13}$$

Assuming that the gravity force is the only body force acting on the fluid, one can express $\underline{F}$ by:

$$\underline{F} = \nabla(-gy_o) \tag{14}$$

where g is the gravitational acceleration and y_o is the vertical coordinate in the nonrotating coordinate system (x_o, y_o, z_o) as shown in Figure 1. It is to be noted that this term is time-dependent in the rotating frame of reference.

Utilizing Equation (14) and the vector identities,

$$\frac{1}{2}\nabla(\underline{V}\cdot\underline{V}) = (\underline{V}\cdot\nabla)\underline{V} + \underline{V} \times (\nabla \times \underline{V}) \tag{15}$$

and

$$-\underline{\Omega} \times (\underline{\Omega} \times \underline{r}) = \frac{1}{2}\nabla|\underline{\Omega} \times \underline{r}|^2, \tag{16}$$

one can express Equation (13) as follows:

$$\nabla\left\{\frac{1}{2}\,\underline{V}\cdot\underline{V} + \frac{p}{\rho} - \frac{1}{2}\,|\underline{\Omega} \times \underline{r}|^2 + gy_o\right\} = -\frac{\partial \underline{V}}{\partial t} + \underline{V} \times (\underline{\omega} + 2\underline{\Omega}) \tag{17}$$

Here, $\underline{\omega}$ is the vorticity in the fluid measured in the moving frame of reference.

Now, consider a propeller rotating at a constant angular velocity, $\underline{\Omega} = -\Omega\underline{i}$ (a right-hand rotation propeller, see Figure 1), in an axisymmetric wake of a ship, where the flow is steady in the rotating frame of reference. The ship wake velocity, $\underline{V}_w$, can be expressed in polar components as:

$$\underline{V}_w = V_x\underline{i} + V_r\underline{e}_r + V_\theta\underline{e}_\theta \tag{18}$$

where V_x, V_r and V_θ are radially varying axial, radial, and tangential components, respectively. It is assumed that the variation of the ship wake velocity in the radial direction is small.

In addition to the ship wake velocity we assume that there exists another axisymmetric disturbance velocity component, $\underline{V}_o$, that is introduced locally by nearby appendages or other lifting surfaces:

$$\underline{V}_o = V_{ox}\underline{i} + V_{or}\underline{e}_r + V_{o\theta}\underline{e}_\theta \tag{19}$$

Then the total velocity, $\underline{V}$, in a cylindrical coordinate system rotating with the propeller can be expressed as follows:

$$\underline{V} = \underline{V}_w + r\Omega\underline{e}_\theta + \underline{V}_p + \underline{V}_o \tag{20}$$

where $\underline{V}_p$ is the perturbation velocity due to the presence of the propeller.

In the rotating coordinate system, the vorticity vector, $\underline{\omega}$, can be expressed as the sum of two terms:

$$\underline{\omega} = \underline{\omega}_r + \underline{\omega}_w \tag{21}$$

where $\underline{\omega}_r$ is the vorticity due to the rotation of the coordinate system and $\underline{\omega}_w$ is the vorticity in the inertial reference frame. From the definition of vorticity, it can be shown that:

$$\underline{\omega}_r = \nabla \times (r\Omega \underline{e}_\theta) = -2\underline{\Omega} \tag{22}$$

If we let $\underline{r} = x\underline{i} + r\underline{e}_r(\theta)$, $|\underline{\Omega} \times \underline{r}|$ term on the left-hand side of Equation (17) will be:

$$|\underline{\Omega} \times \underline{r}| = r\Omega \tag{23}$$

Substituting Equations (21) to (23) into Equation (17) with the assumption of the steady flow, we have:

$$\nabla \left\{ \frac{1}{2} \underline{V} \cdot \underline{V} + \frac{p}{\rho} - \frac{1}{2} (r\Omega)^2 + gy_o \right\} = \underline{V} \times \underline{\omega}_w \tag{24}$$

By integrating Equation (24) along a path in the flow between two arbitrary points, A and B, we obtain the Bernoulli equation:

$$H_B - H_A = \int_A^B (\underline{V} \times \underline{\omega}_w) \cdot d\underline{r} \tag{25}$$

where $H(\underline{r},t)$ is sometimes called the Bernoulli head and is defined by:

$$H(\underline{r},t) = \frac{1}{2} \underline{V} \cdot \underline{V} + \frac{p}{\rho} - \frac{1}{2} (r\Omega)^2 + gy_o \tag{26}$$

If we take the integral path $d\underline{r}$ along a streamline or a vortex line, i.e., parallel to $\underline{V}$ or $\underline{\omega}_w$, respectively, the integral in Equation (25) vanishes since the dot product in Equation (25) is equal to zero. It then follows that the Bernoulli head is constant along a streamline or a vortex line.

By taking a reference point, A, as a point along the streamline far upstream of the propeller where the propeller perturbation velocity, $\underline{V}_p$, and the other

disturbance velocity, $\underline{V}_o$, are negligibly small, the Bernoulli constant, H_A, will be:

$$H_A = \left[\frac{1}{2} V_x^2 + \frac{p}{\rho} + gy_o\right]_A \tag{27}$$

Then the pressure at an arbitrary point in the fluid can be expressed as:

$$p = -\frac{1}{2}\rho\left\{\underline{V}\cdot\underline{V} - (V_x)_A^2 - r^2\Omega^2\right\} - \rho g(y_o - y_{oA}) + p_A \tag{28}$$

where $\underline{V} = \underline{V}_w + r\Omega\underline{e}_\theta + \underline{V}_p + \underline{V}_o$, and the subscript A indicates a point on the same streamline (or vortex line) where the pressure is computed. The effect of gravity, $-\rho g(y_o - y_{oA})$ in Equation (28) gives rise to a once-per-revolution periodic variation in the pressure in the rotating coordinate system. Since this term does not contribute to the mean pressure and the loading, it is not considered in the present study. However, this term may be important when cavitation inception is of interest.

For a uniform onset flow (potential flow) with only an axial component and with no other disturbance than the propeller itself, i.e., the flow condition applicable to all the experimental measurements correlated in this report, the pressure equation becomes even simpler:

$$p = -\frac{1}{2}\rho\left\{\underline{V}\cdot\underline{V} - V_x^2 - r^2\Omega^2\right\} + p_\infty \tag{29}$$

where $\underline{V} = V_x\underline{i} + r\Omega\underline{e}_\theta + \underline{V}_p$, and p_∞ is the known pressure far upstream. In this case, the Bernoulli head is constant everywhere in the fluid since there is no vorticity in the flow (see Equation (24)).

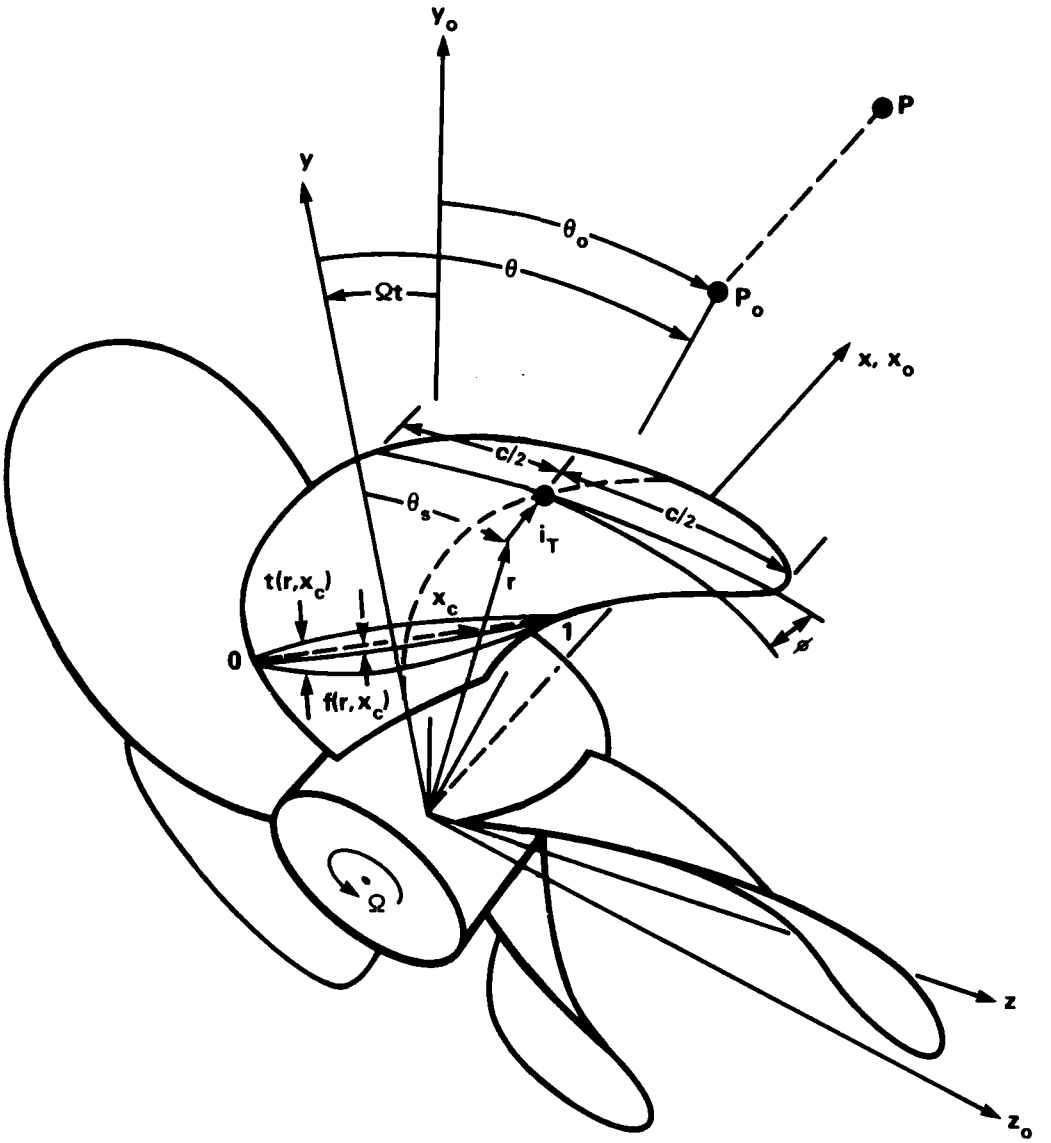

Figure 1 - Fixed and Rotating Coordinate Systems for a Right-Hand-Rotation Propeller

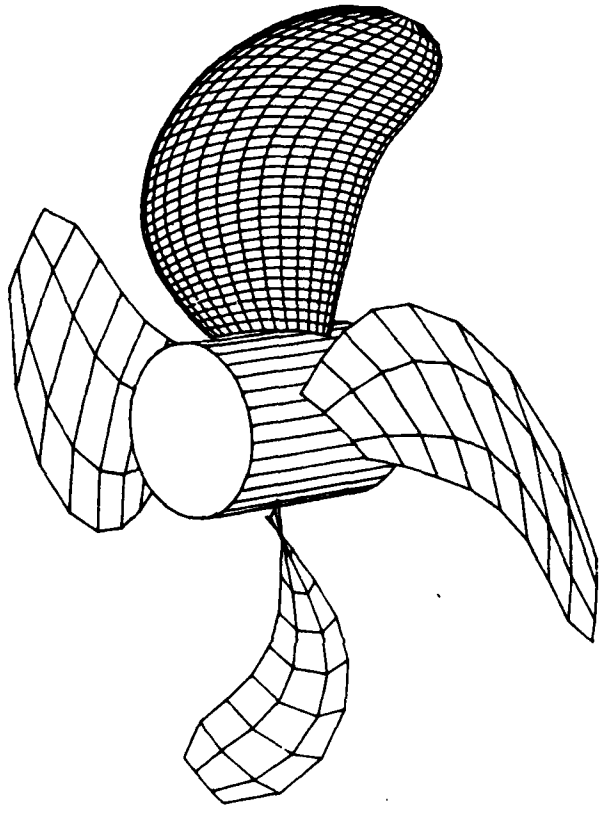

Figure 2 - Discretization of Blade Singularities

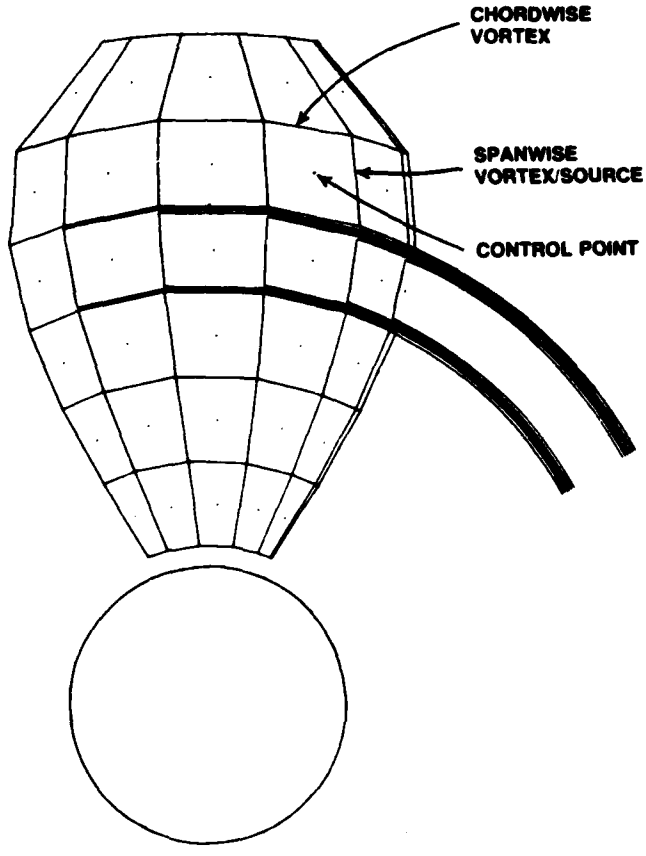

Figure 3 - Horseshoe Vortices on Blade and in Wake

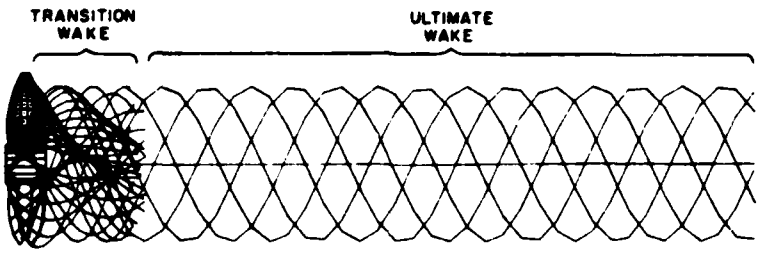

Figure 4 - Trailing Wake Geometry after Wake Alignment

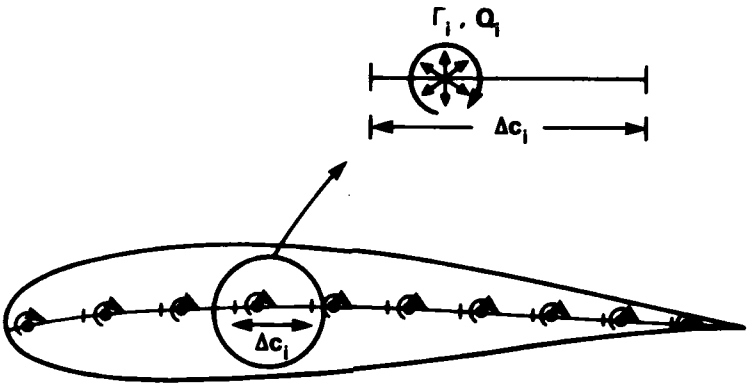

Γ : **DISCRETE BOUND VORTEX STRENGTH**

Q : DISCRETE SOURCE STRENGTH

γ : **DISTRIBUTED BOUND VORTEX STRENGTH**

$$\gamma_i = \frac{\Gamma_i}{\Delta c_i}$$

q : DISTRIBUTED SOURCE STRENGTH

$$q_i = \frac{Q_i}{\Delta c_i}$$

Figure 5 - Discrete Singularity Distribution for Two-Dimensional Airfoil Section

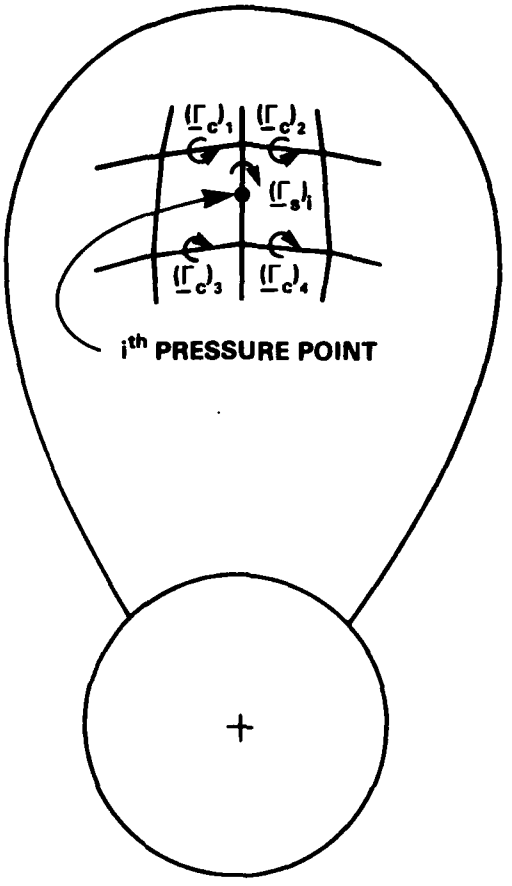

$\underline{\Gamma}_s$: SPANWISE DISCRETE VORTEX

$\underline{\Gamma}_c$: CHORDWISE DISCRETE VORTEX

$\underline{\gamma}_s$: SPANWISE DISTRIBUTED VORTEX, $(\underline{\gamma}_s)_i = \dfrac{(\underline{\Gamma}_s)_i}{\Delta c_i}$

$\underline{\gamma}_c$: CHORDWISE DISTRIBUTED VORTEX, $(\underline{\gamma}_c)_i = \dfrac{1}{4} \sum_{n=1}^{4} \dfrac{(\underline{\Gamma}_c)_n}{\Delta r_n}$

$\underline{\gamma}_i$: TOTAL DISTRIBUTED VORTEX AT i^{th} PRESSURE POINT

$\underline{\gamma}_i = (\underline{\gamma}_s)_i + (\underline{\gamma}_c)_i$

Figure 6 - Schematic Representation of the Effect of Chordwise Vortices on the i^{th} Pressure Point

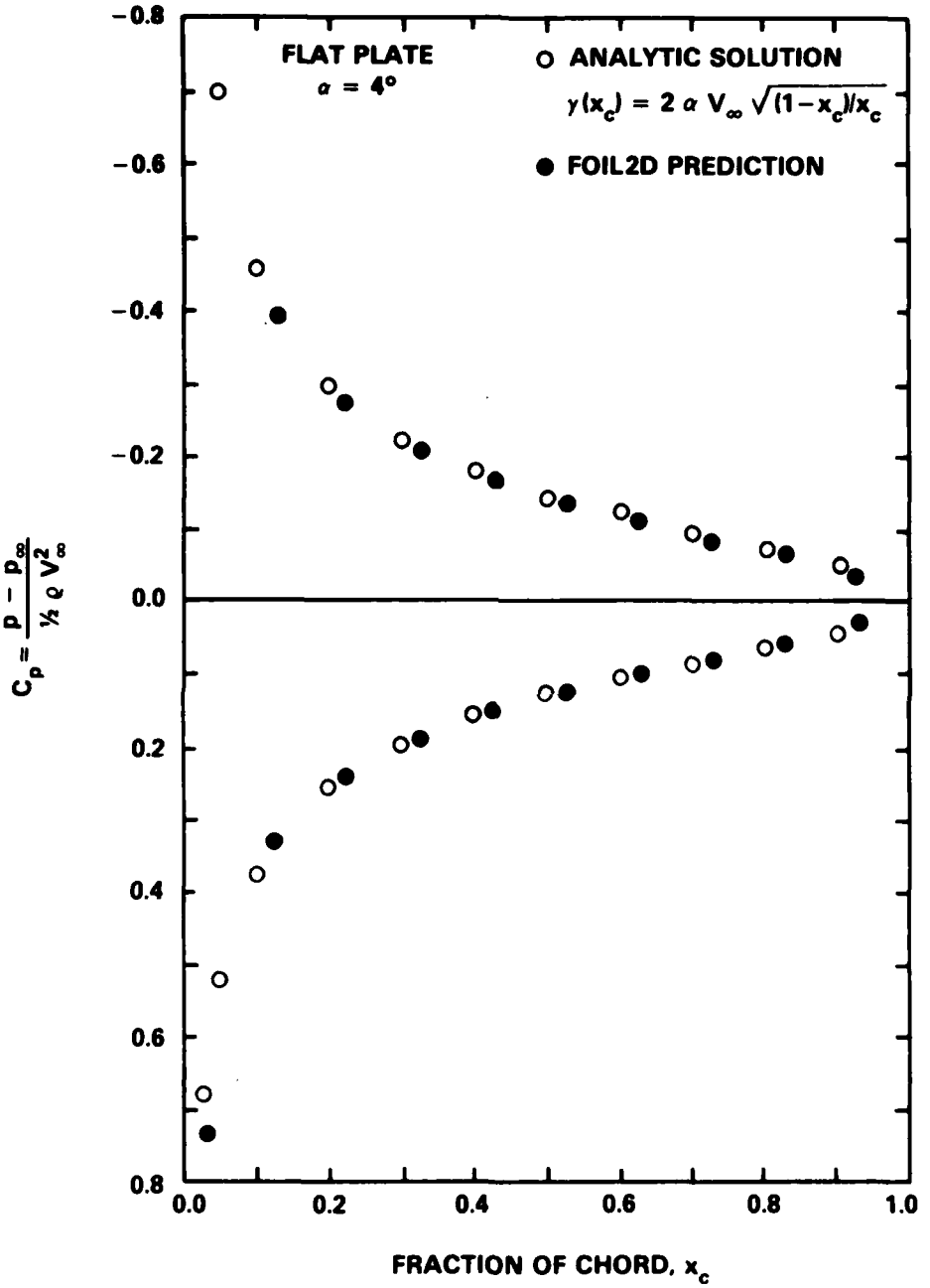

Figure 7 - Pressure Distribution on Flat Plate at α = 4 Degrees

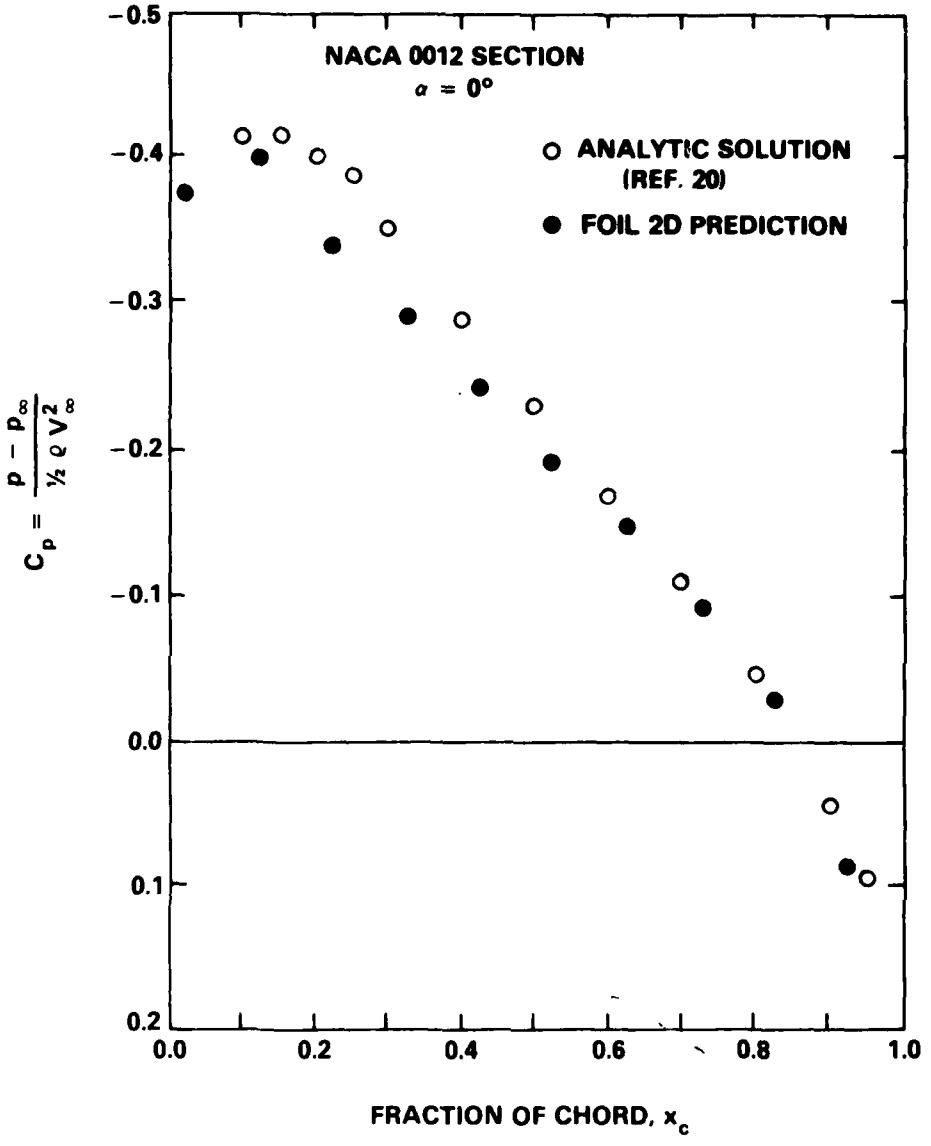

Figure 8 - Pressure Distribution on NACA 0012 Section at α = 0 Degrees

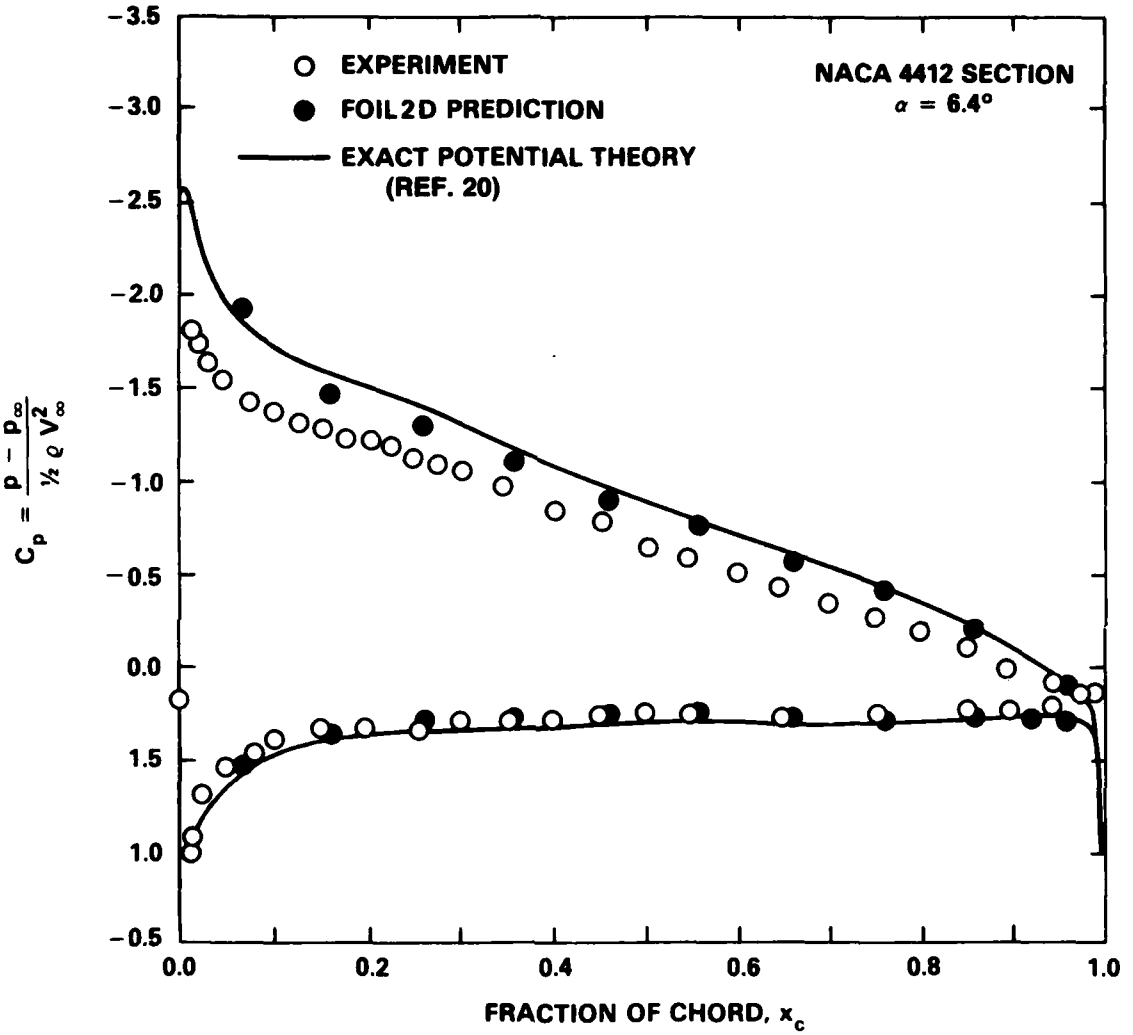

Figure 9 - Pressure Distribution on NACA 4412 Section at α = 6.4 Degrees

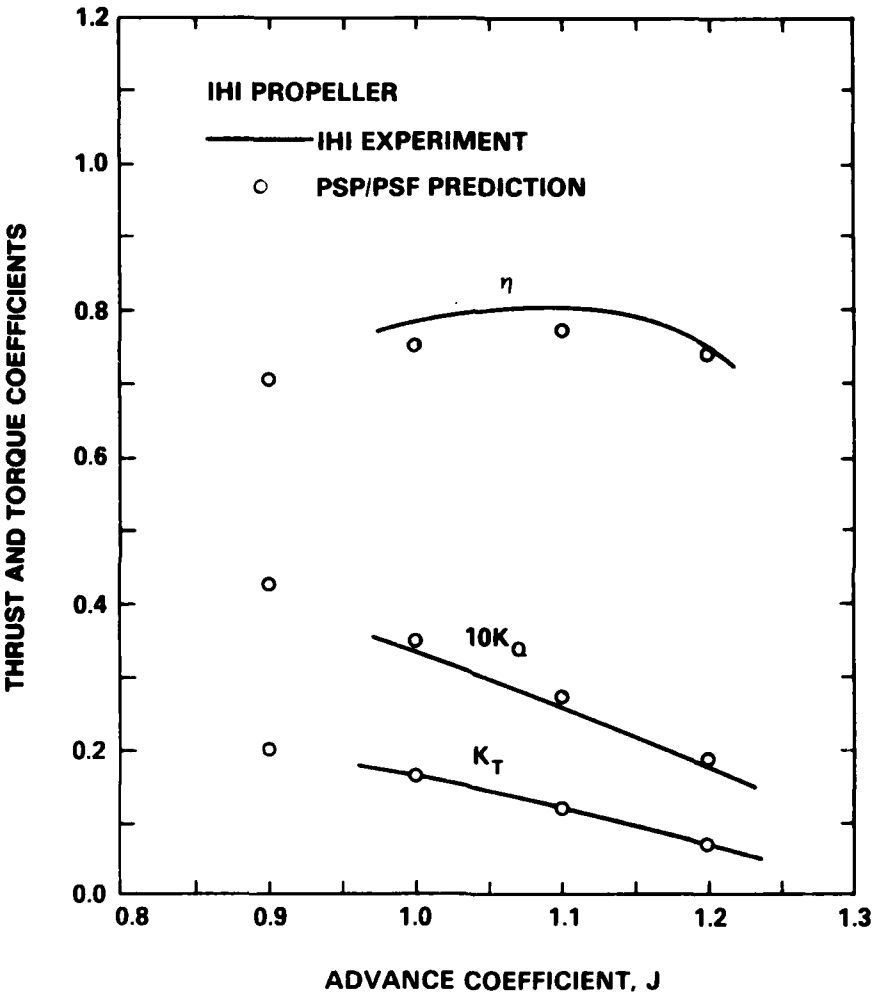

Figure 10 - Open-Water Performance of IHI Model Propeller MP 282

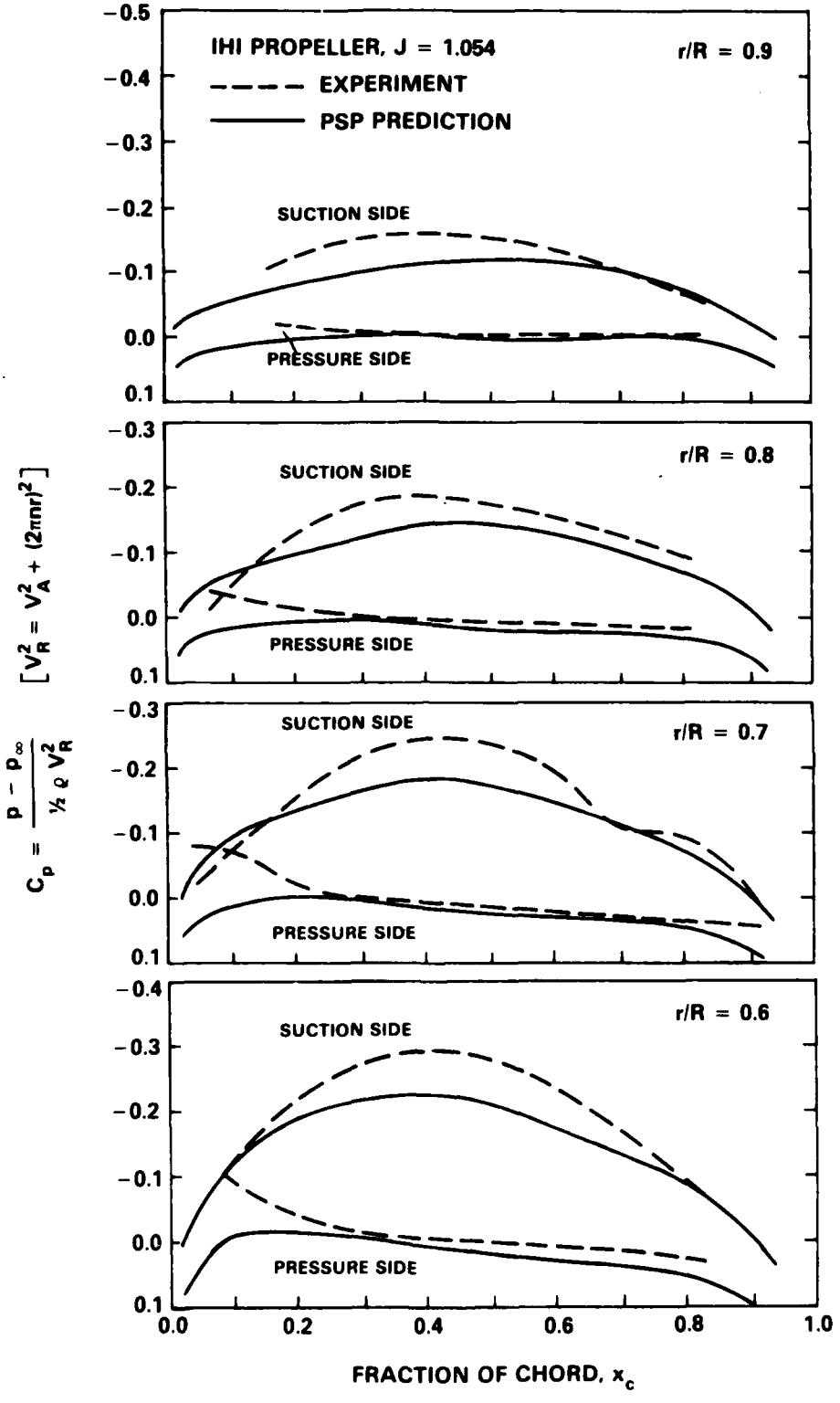

Figure 11 - Pressure Distribution on IHI Model Propeller MP 282 at J = 1.054

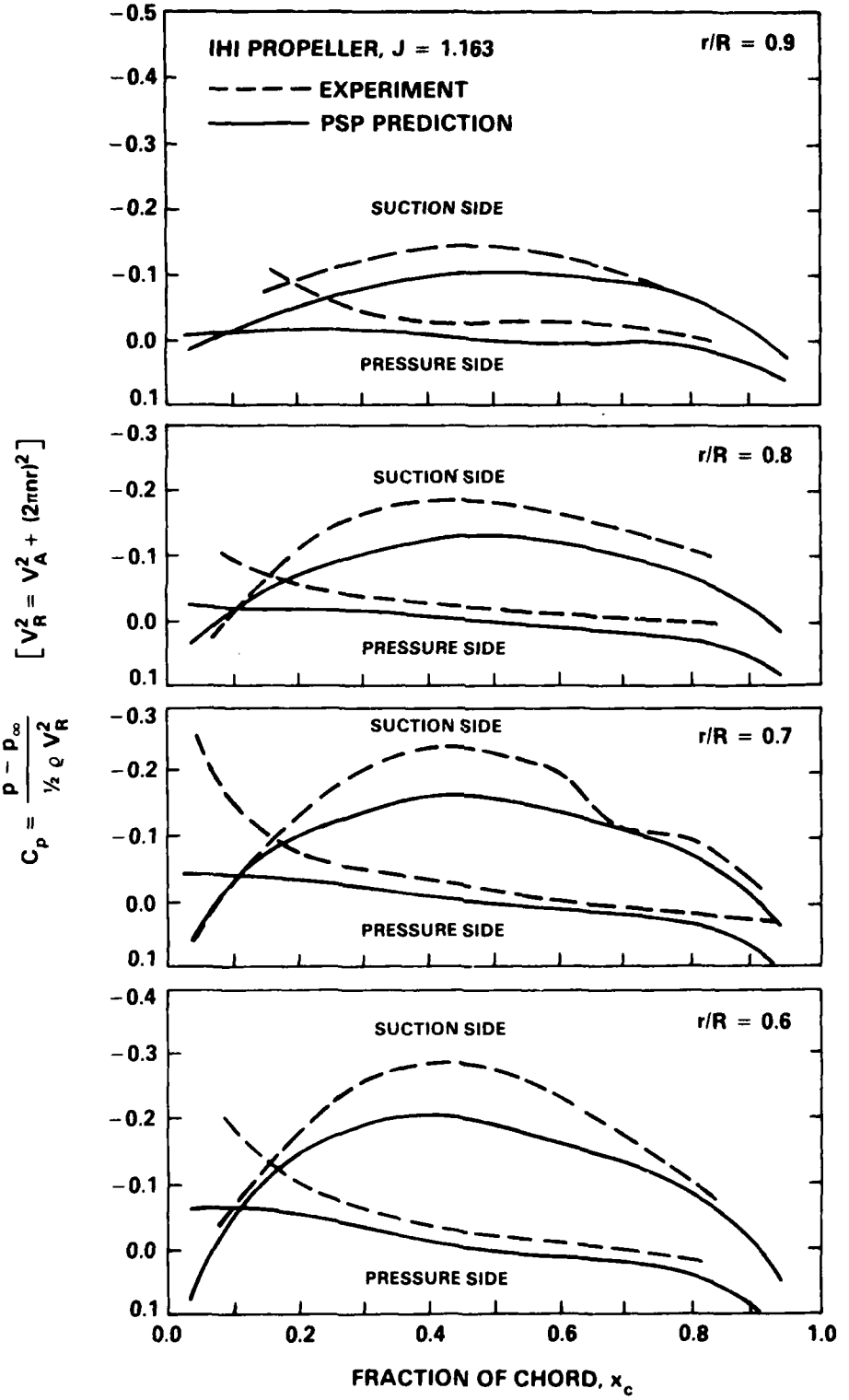

Figure 12 - Pressure Distribution on IHI Model Propeller MP 282 at J = 1.163

SUCTION SIDE PRESSURE SIDE

$R_n = 1.1 \times 10^6$, J = 1.14

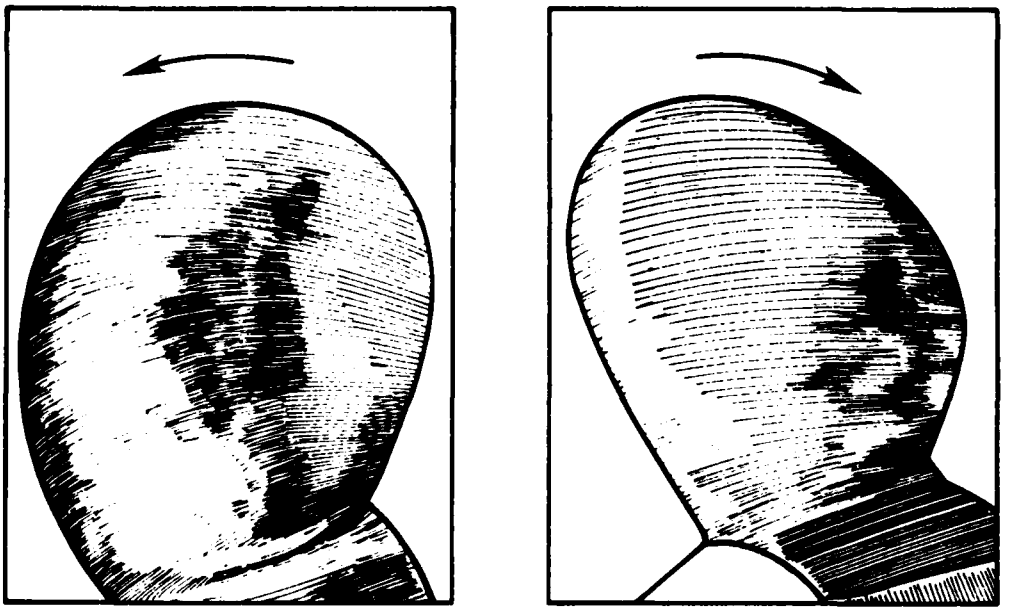

SUCTION SIDE PRESSURE SIDE

R_n 2.6 · 10^6, J 1.15

Figure 13 - Surface Flow Patterns by Oil-Film Test on IHI Model Propeller MP 282

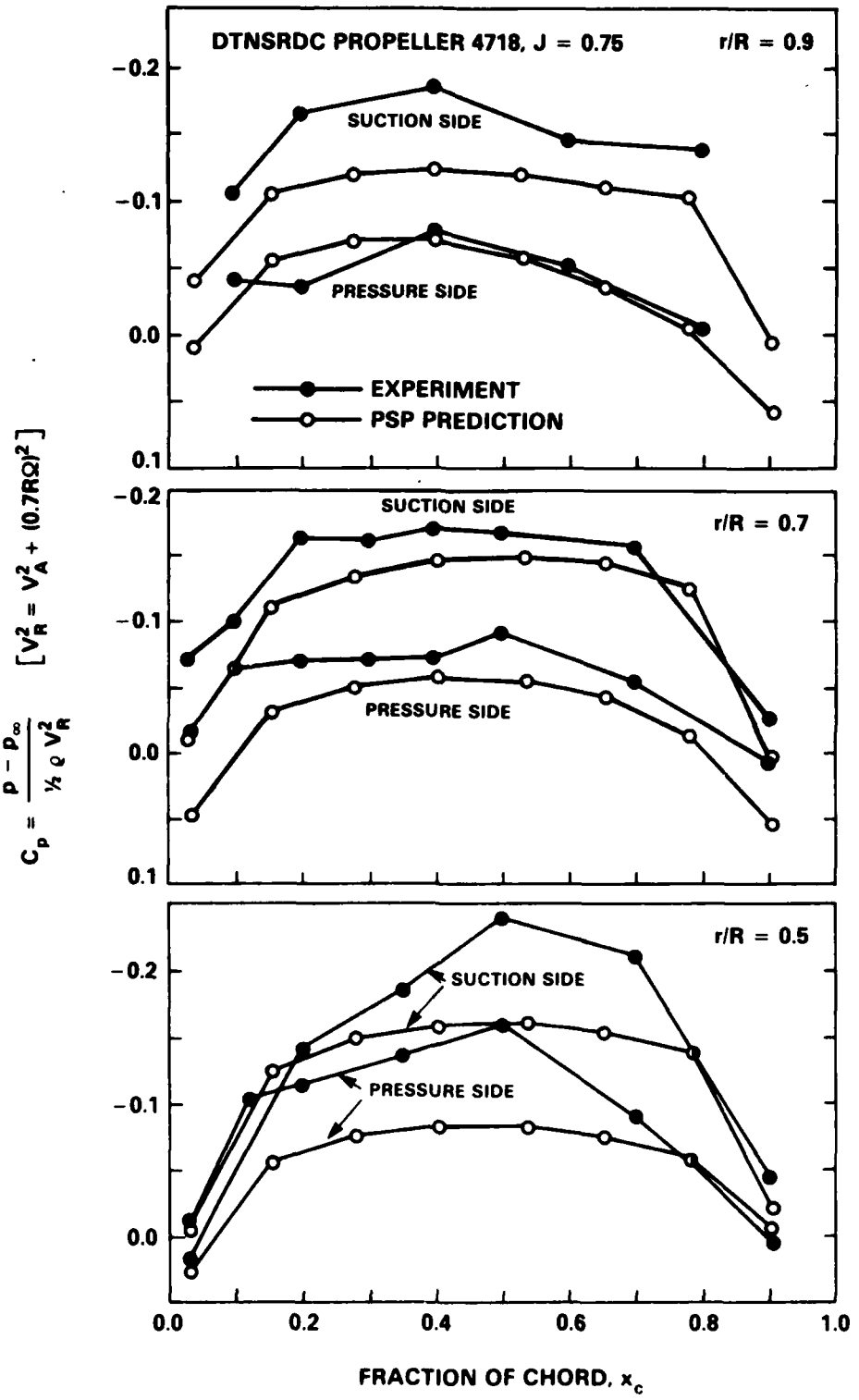

Figure 14 - Pressure Distribution on DTNSRDC Propeller 4718 at J = 0.75

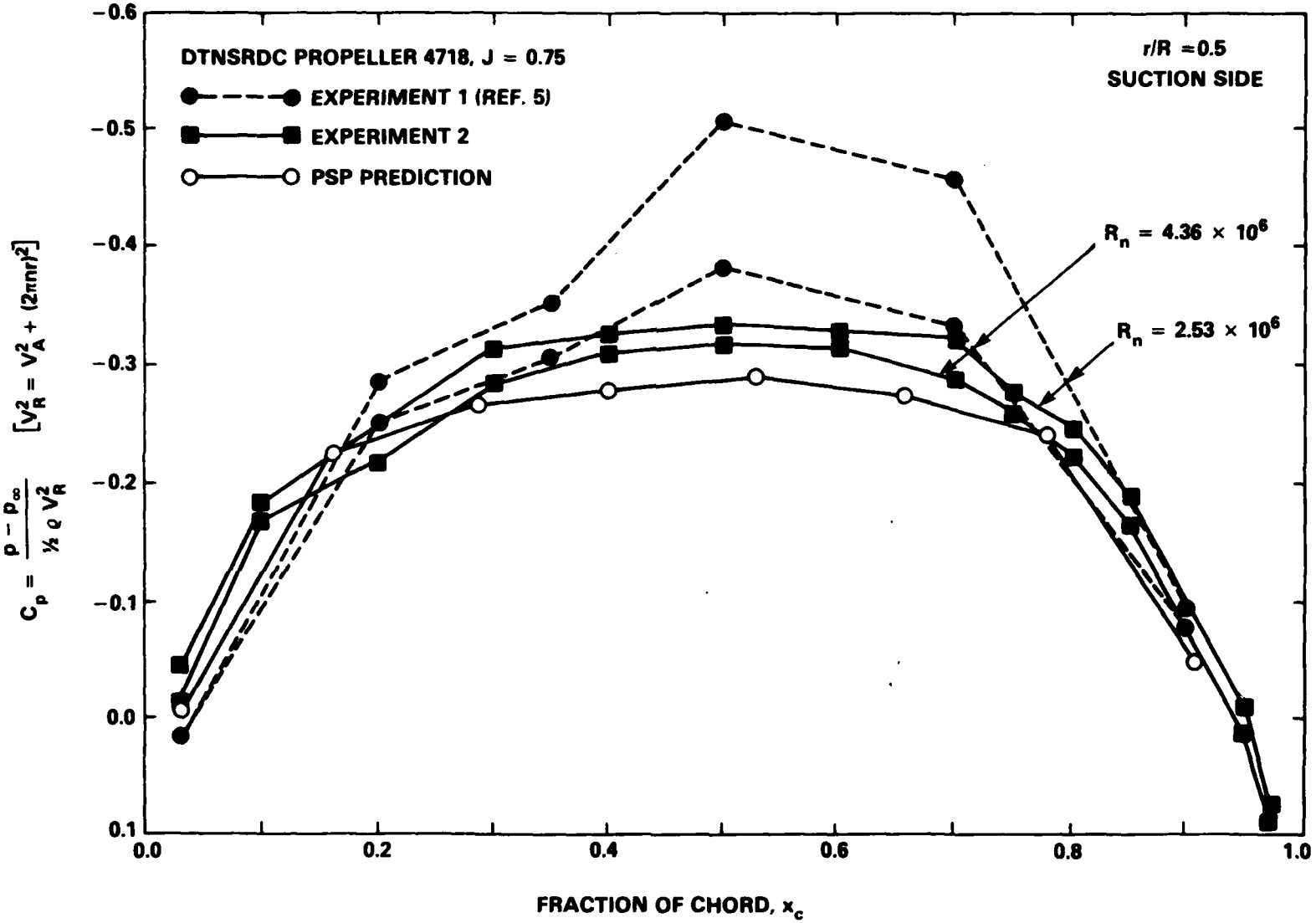

Figure 15 - Pressure Distribution on Suction Side of DTNSRDC Propeller 4718 at r/R = 0.5: Comparison of Prediction and Two Sets of Experiments

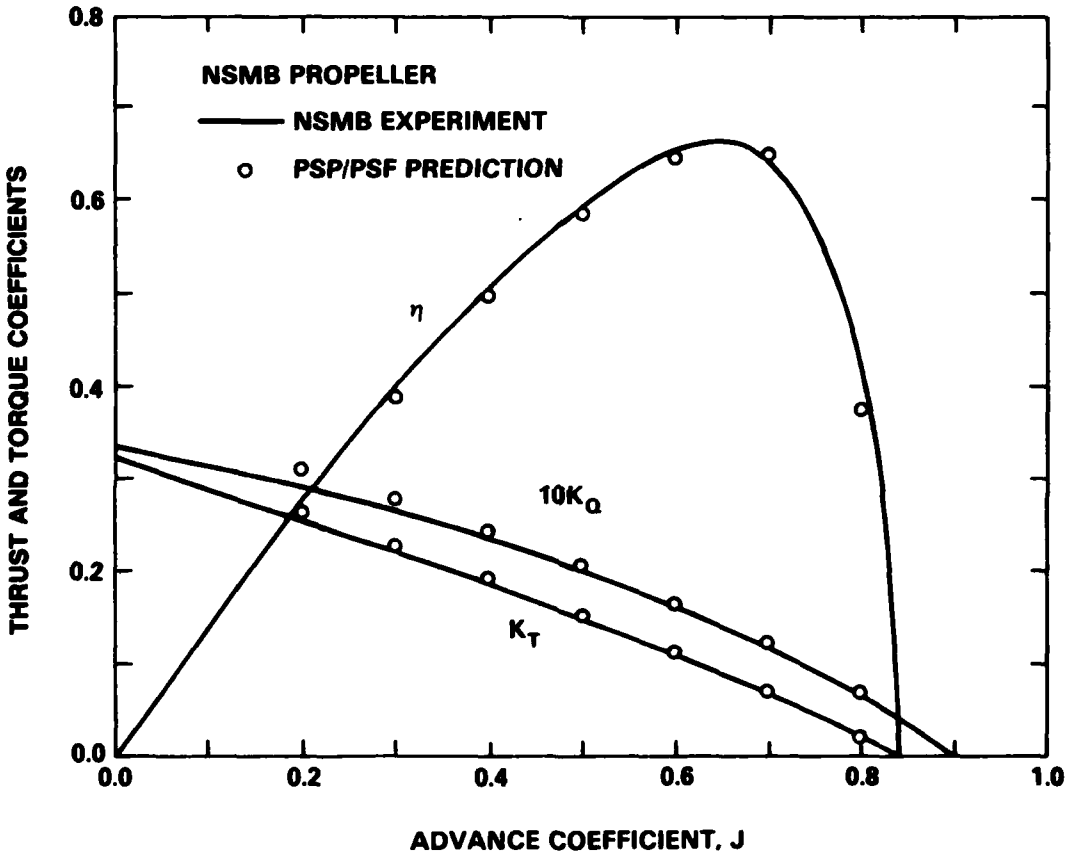

Figure 16 - Open-Water Performance of NSMB Model Propeller

Figure 17 - Pressure Distribution on NSMB Propeller at J = 0.4

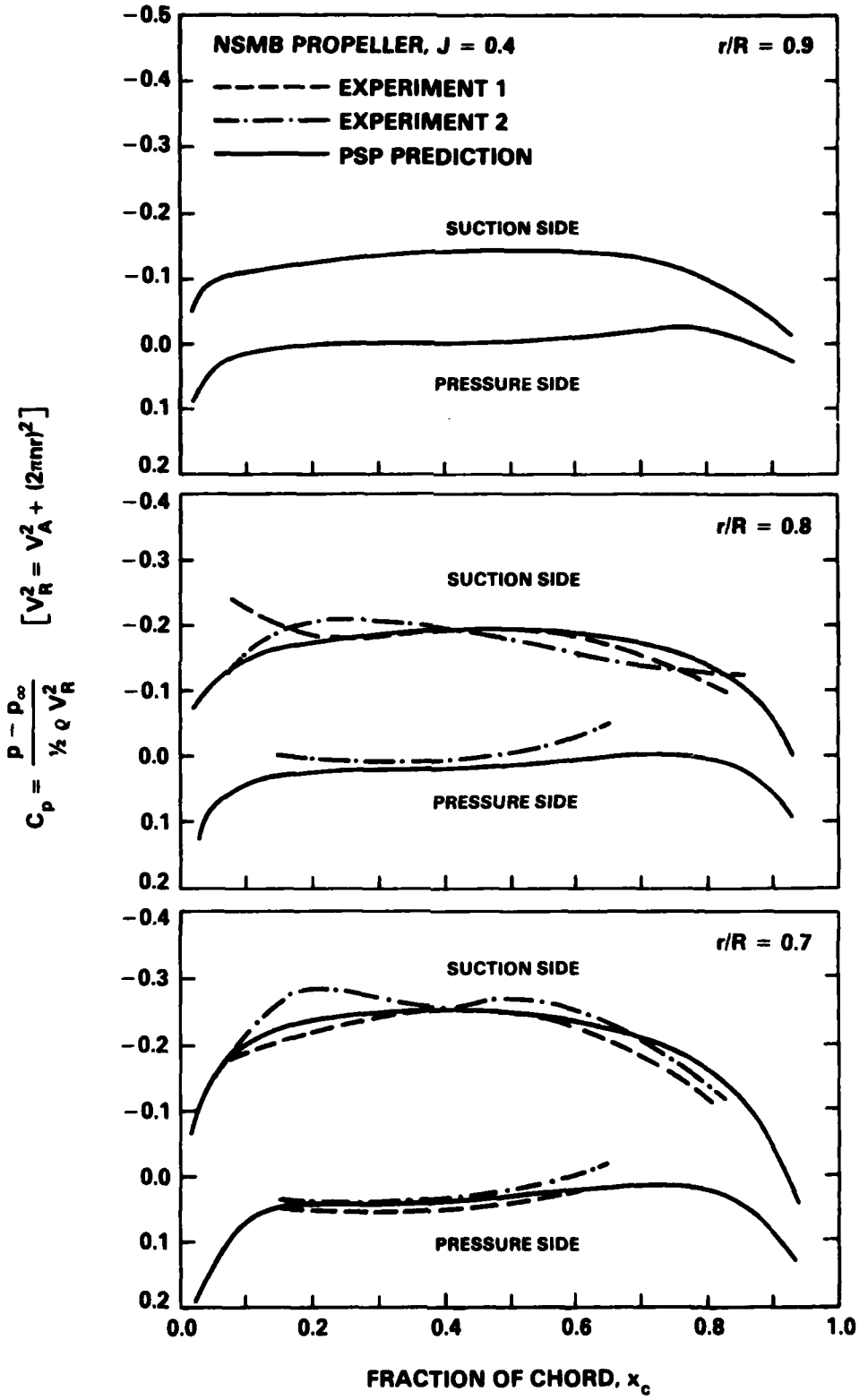

Figure 17 (Continued)

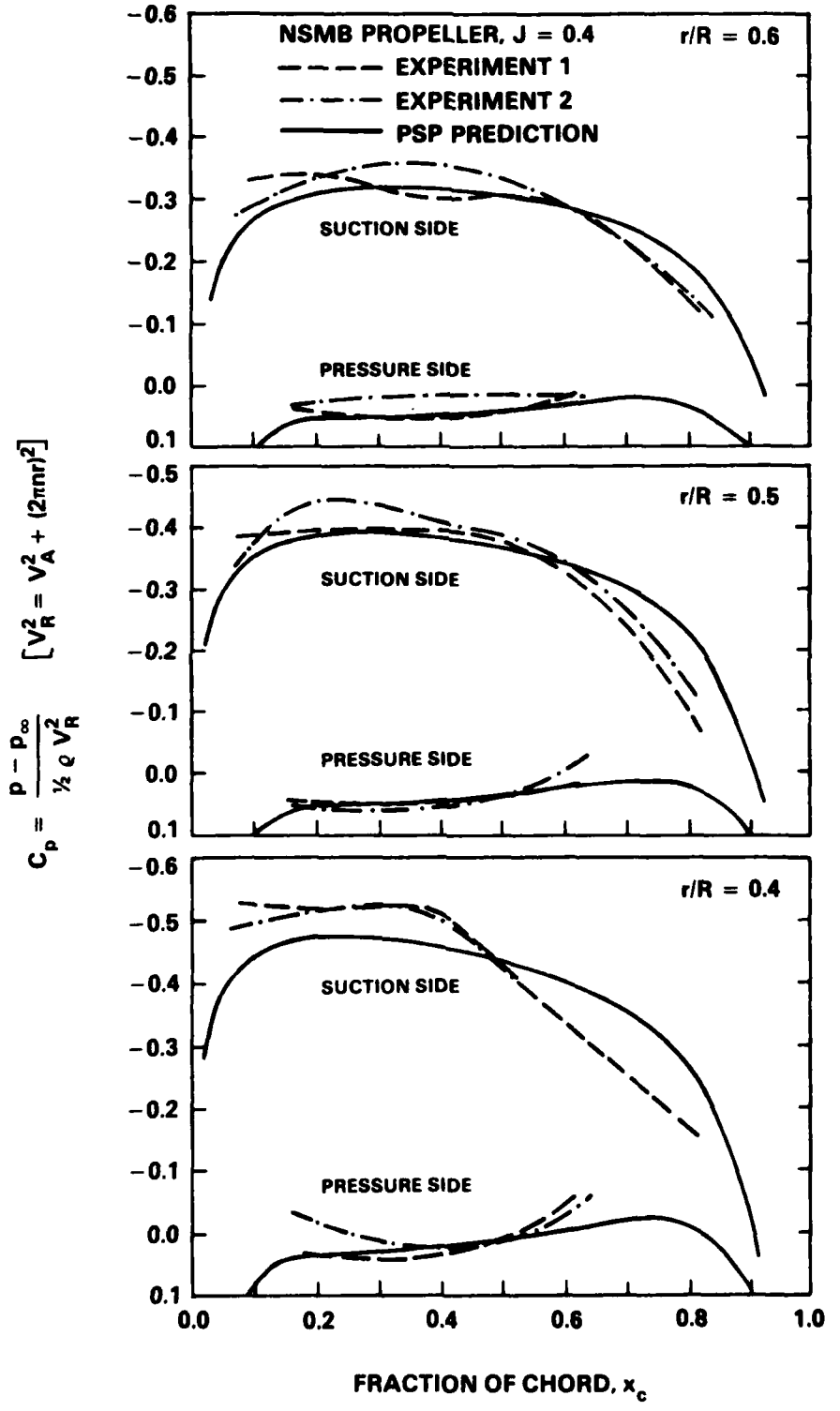

Figure 18 - Pressure Distribution on NSMB Propeller at J = 0.6

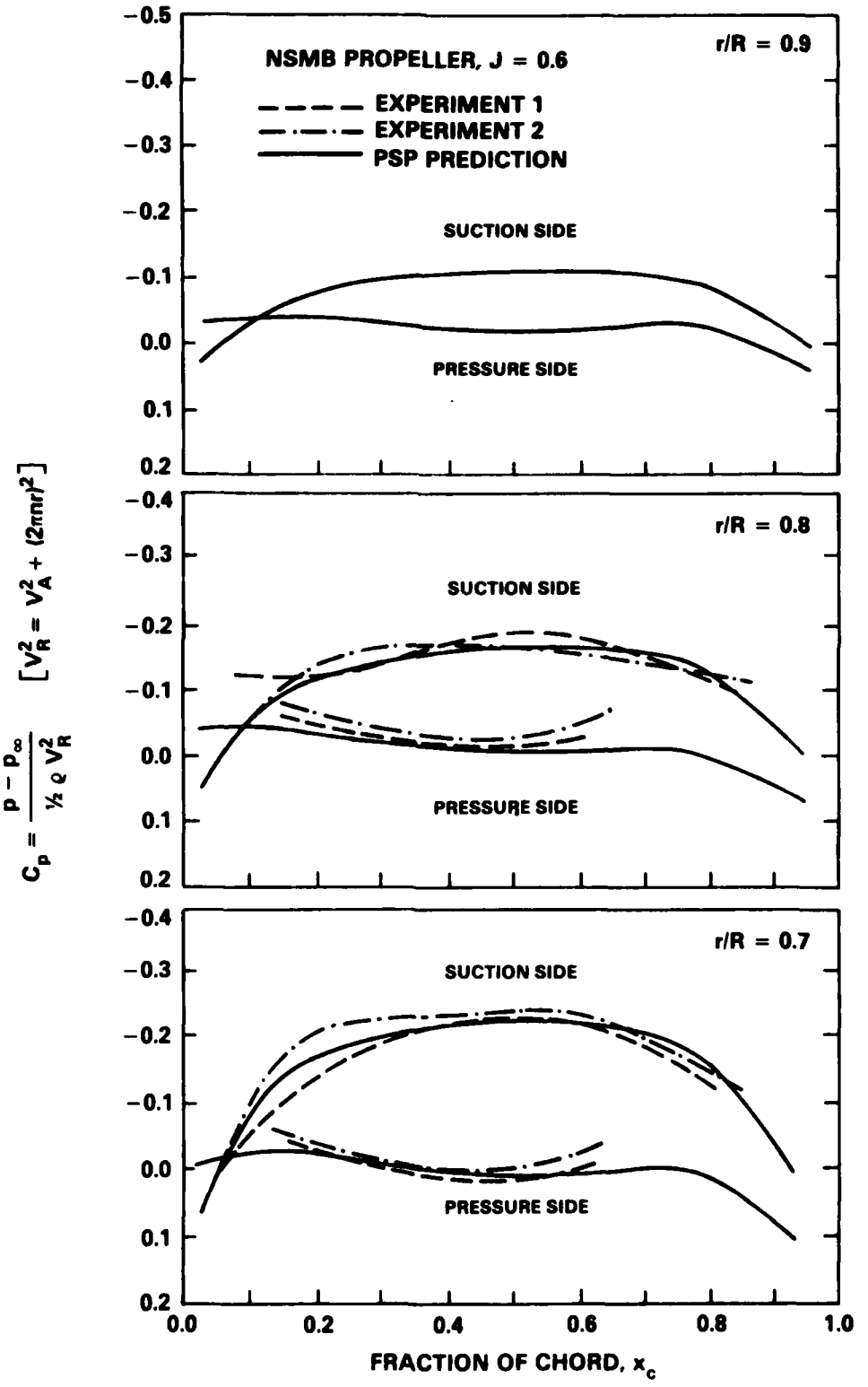

Figure 18 (Continued)

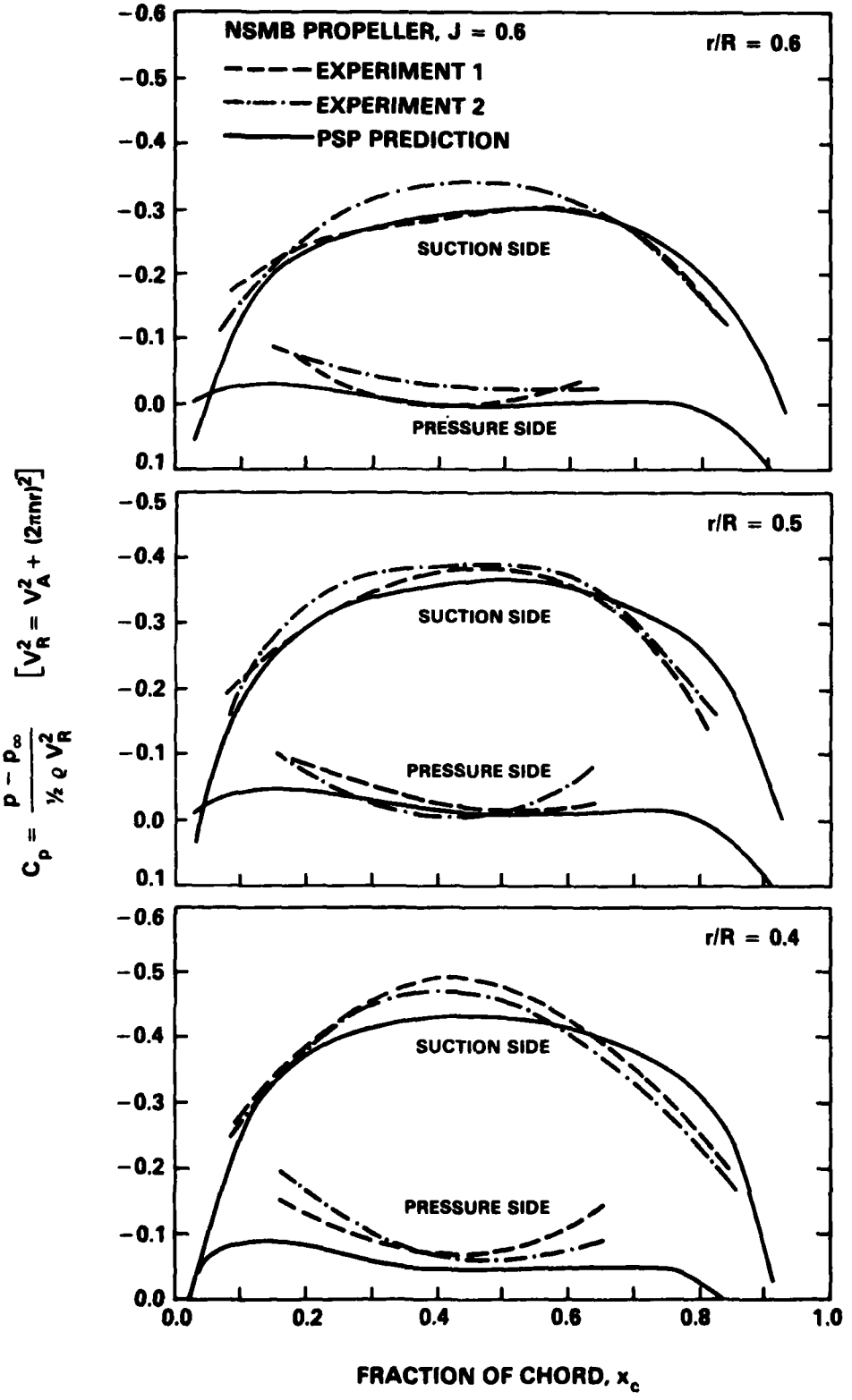

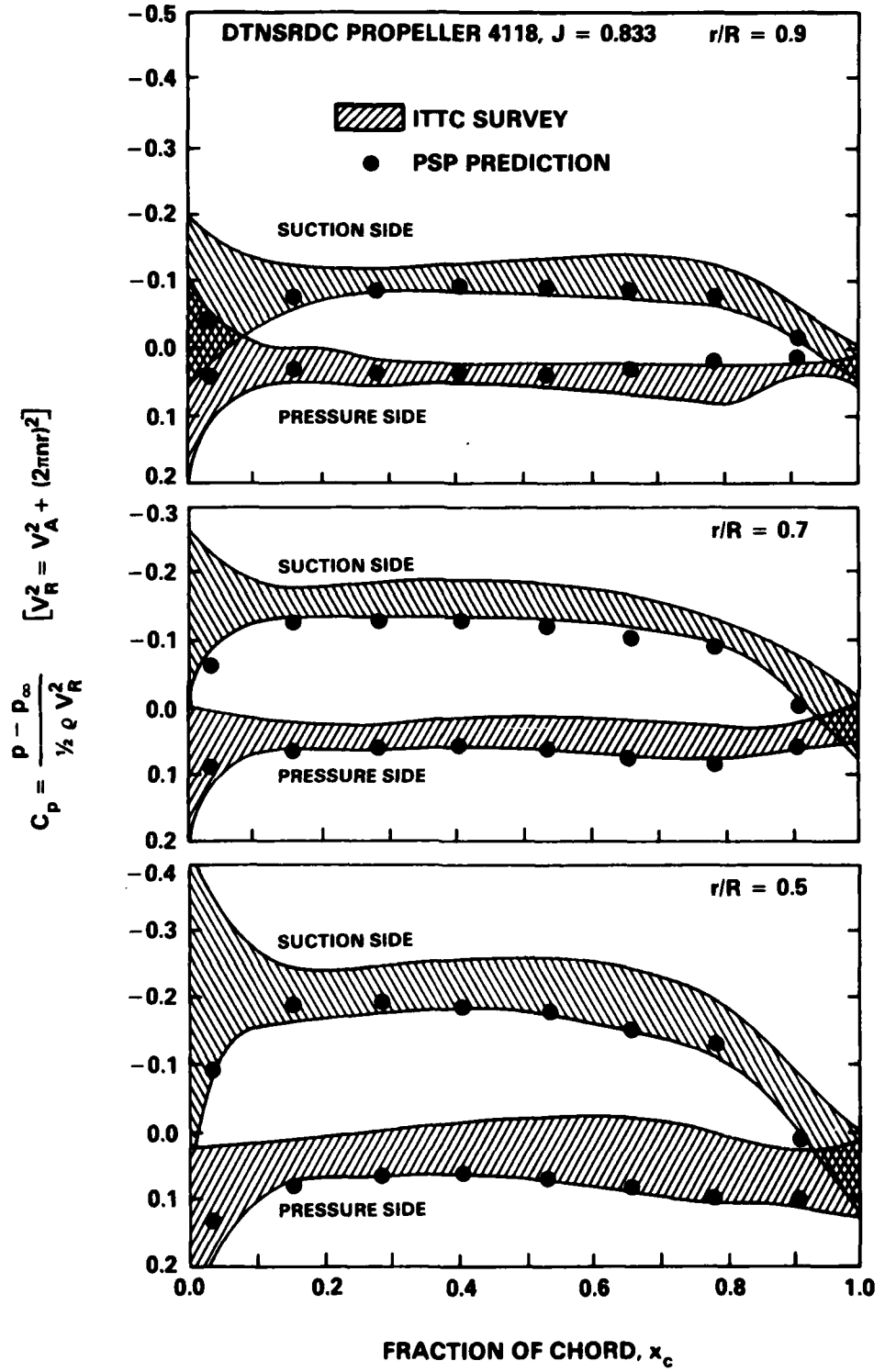

Figure 19 - Pressure Distribution on DTNSRDC Propeller 4118 at J = 0.833: Comparison with ITTC Propeller Committee Survey

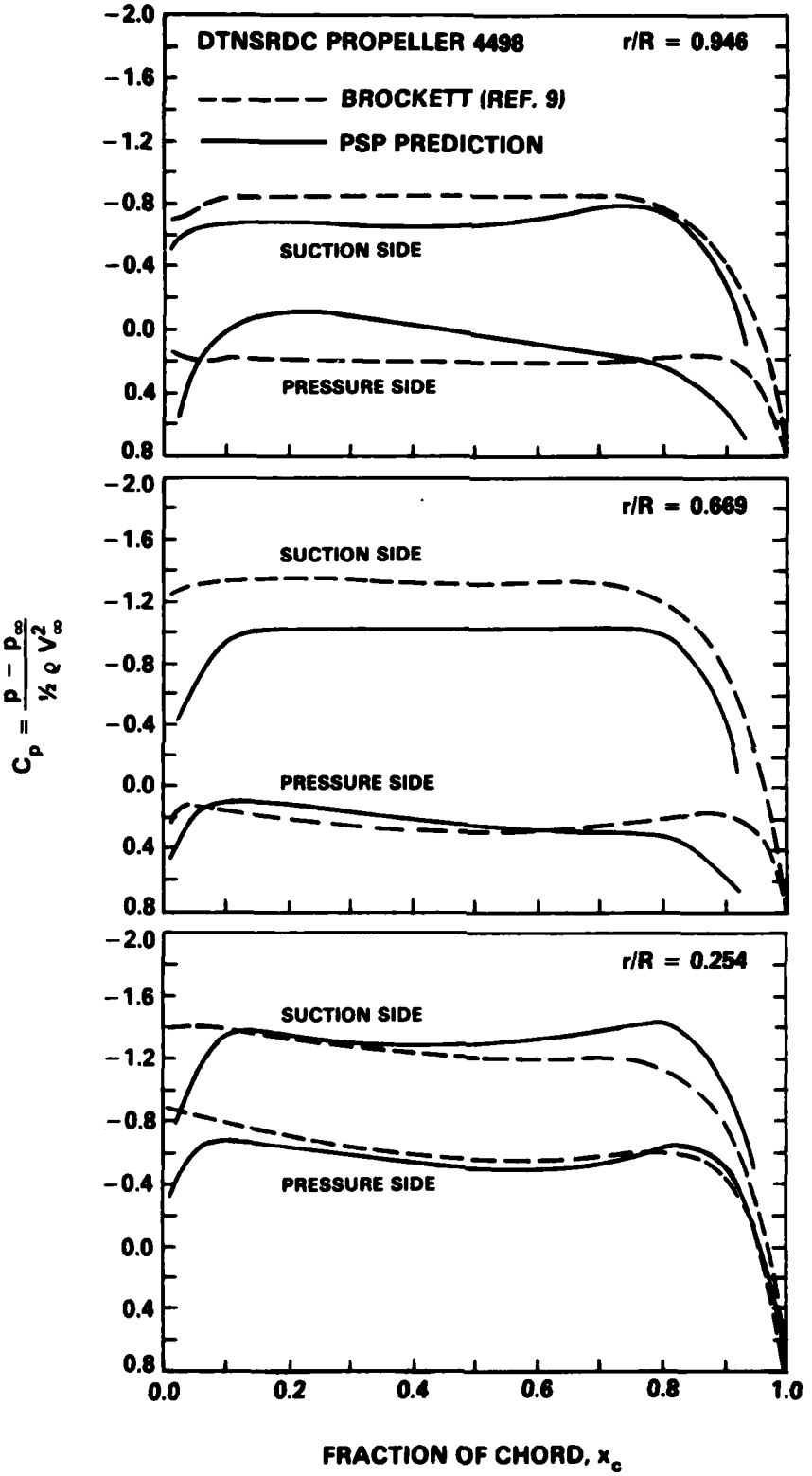

Figure 20 - Pressure Distribution on DTNSRDC Propeller 4498 at J = 0.888

TABLE 1 - PROPELLER GEOMETRIC CHARACTERISTICS

Propeller Identification	IHI MP 282	DTNSRDC 4718	NSMB Propeller	DTNSRDC 4118	DTNSRDC 4498
Number of Blades, Z	4	3	4	3	5
Expanded Area Ratio (EAR), A_E/A_o	0.639	0.44	0.6	0.6	0.727
Diameter; D(m)	0.95	0.61	0.48	0.305	0.305
Pitch-Diameter Ratio (P/D) at r/R = 0.7	1.24	0.888	0.795	1.077	1.16
Design Advance Coefficient, J	--	0.751	--	0.833	0.888
Tip Skew, θ_s (Degrees)	6.67	20.0	0.0	0.0	72.0

INITIAL DISTRIBUTION

Copies	
1	ARMY CHIEF OF RES & DEV
1	AER&DL
3	CHONR
	1 Code 438
	1 Lib
	1 Lee
4	ONR BOSTON
4	ONR CHICAGO
4	ONR LONDON, ENGLAND
1	NRL
2	USNA
	1 Lib
	1 Johnson
1	NAVPGSCOL Lib
1	NROTC & NAVADMINU, MIT
1	NADC
5	NOSC
	1 1311 Lib
	1 6005
	1 13111 Lib
	1 2501/Hoyt
	1 Nelson
1	NSWC
43	NAVSEA
	3 SEA 05H
	5 SEA 05R
	1 SEA 55
	3 SEA 55D
	3 SEA 55N
	1 SEA 55W
	3 SEA 56D
	1 SEA 56X
	3 SEA 56X1
	1 SEA 56X2
	3 SEA 56X4
	1 SEA 56X5
	1 SEA 56XP
	1 PMS-378
	1 PMS-380
	1 PMS-381
	1 PMS-383

Copies	
	NAVSEA (Continued)
	1 PMS-389
	1 PMS-391
	1 PMS-392
	1 PMS-393
	1 PMS-397
	1 PMS-399
	1 PMS-400
	1 SEA Tech Rep Bath, England
	2 DET NORFOLK (Sec 6660)
2	MMA
	1 Lib
	1 Maritime Res Cen
1	NAVFAC 032C
1	MILITARY SEALIFT COMMAND (M-4EX)
1	NAVSHIPYD/PTSMH
1	NAVSHIPYD/PHILA
1	NAVSHIPYD/NORVA
1	NAVSHIPYD/CHASN
1	NAVSHIPYD/LBEACH
1	NAVSHIPYD/MARE
1	NAVSHIPYD/PUGET
1	NAVSHIPYD/PEARL
12	DTIC
2	HQS COGARD
1	US COAST GUARD (G-ENE-4A)
1	LC/SCI & TECH DIV
8	MARAD
	1 DIV SHIP DES
	1 COORD RES
	1 Shubert
	1 Falls
	1 Dashnaw
	1 Hammer
	1 Lasky
	1 Siebold
2	NASA STIF
	1 DIR RES

Copies

1 NSF ENGR DIV/LIB

1 DOT Lib

1 U BRIDGEPORT/URAM

2 U CAL BERKELEY/DEPT NAME
- 1 NAME Lib
- 1 Webster

1 U CAL SAN DIEGO/Ellis

2 UC SCRIPPS
- 1 Pollack
- 1 Silverman

1 U MARYLAND/GLENN MARTIN INST

1 U MISSISSIPPI DEPT OF M.E.
- 1 Fox

4 CIT
- 1 AERO Lib
- 1 Acosta
- 1 Plesset
- 1 Wu

1 CATHOLIC U

1 COLORADO STATE U/Albertson

1 U CONNECTICUT/Scottron

1 CORNELL U/Sears

1 FLORIDA ATLANTIC U OE Lib

1 HARVARD U/McKay Lib

2 U HAWAII/Bretschneider

1 U ILLINOIS/Robertson

5 U IOWA
- 1 Lib
- 1 IHR/Kennedy
- 1 IHR/Landweber
- 1 IHR/Stern
- 1 IHR/Patel

1 JOHNS HOPKINS U/Phillips

1 U KANSAS CIV ENGR/Lib

1 KANSAS ST U ENGR EXP/Lib

1 LEHIGH U/FRITZ ENGR LAB Lib

4 U MICHIGAN/DEPT NAME
- 1 NAME Lib
- 1 Brockett

Copies

2 U MICHIGAN/DEPT NAME (Continued)
- 1 Parsons
- 1 Vorus

3 MIT
- 1 BARKER ENGR Lib
- 2 OCEAN ENGR/Kerwin

3 U MINNESOTA SAFHL
- 1 Killen
- 1 Song
- 1 Wetzel

3 STATE U MARITIME COLL
- 1 ARL Lib
- 1 ENGR DEPT
- 1 INST MATH SCI

1 NOTRE DAME ENGR Lib

5 PENN STATE U ARL
- 1 Lib
- 1 Henderson
- 1 Gearhart
- 1 Parkin
- 1 Thompson

1 PRINCETON U/Mellor

1 RENSSELAER/DEPT MATH

1 ST JOHNS U

1 VIRGINIA TECH

2 SWRI
- 1 APPLIED MECH REVIEW
- 1 Abramson

1 BOEING ADV AMR SYS DIV

1 BB&N/Jackson

1 BREWER ENGR LAB

1 CAMBRIDGE ACOUS/Junger

1 CALSPAN, INC/Ritter

1 STANFORD U/Ashley

1 STANFORD RES INST Lib

4 SIT DAVIDSON LAB
- 1 Lib
- 1 Breslin
- 1 Tsakonas
- 1 McKee

Copies	
1	TEXAS U ARL Lib
1	UTAH STATE U/Jeppson
2	VPI/DEPT AERO & OCEAN ENGR 1 Schetz 1 Kaplan
2	WEBB INST 1 Ward 1 Hadler
1	WHOI OCEAN ENGR DEPT
1	WPI ALDEN HYDR LAB Lib
1	ASME/RES COMM INFO
1	ASNE
1	SNAME/Tech Lib
1	AERO JET-GENERAL/Beckwith
1	ALLIS CHALMERS, YORK, PA
1	AVCO LYCOMING
1	BAKER MANUFACTURING
2	BATH IRON WORKS CORP 1 Hansen 1 FFG7 PROJECT OFFICE
1	BETHLEHEM STEEL/Sparrows Point
1	BIRD-JOHNSON CO/Norton
1	DOUGLAS AIRCRAFT/Lib
2	EXXON RES DIV 1 Lib 1 Fitzgerald
1	FRIEDE & GOLDMAN/Michel
1	GENERAL DYNAMICS, EB/Boatwright
1	GIBBS & COX/Lib
1	ROSENBLATT & SON/Lib
1	GRUMMAN AEROSPACE/Carl
1	TRACOR HYDRONAUTICS/Lib
1	INGALLS SHIPBUILDING
1	INST FOR DEFENSE ANAL
1	ITEK VIDYA
1	LIPS DURAN/Kress

Copies	
1	LITTLETON R & ENGR CORP/Reed
1	LITTON INDUSTRIES
1	LOCKHEED, SUNNYVALE/Waid
2	MCDONNEL DOUGLAS, LONG BEACH 1 Cebeci 1 Hess
1	MARITECH, INC/Vassilopoulis
2	HRA, INC 1 Cox 1 Scherer
1	NATIONAL STEEL & SHIPBUILDING
1	NEWPORT NEWS SHIPBUILDING/Lib
1	NIELSEN ENGR/Spangler
1	NKF ASSOCIATES/Noonan
1	NAR SPACE/Ujihara
11	ORI, INC 10 Kobayashi 1 Lin
2	ATLANTIC APPLIED RESEARCH 1 Brown 1 Greeley
1	PROPULSION DYNAMICS, INC
1	PROPULSION SYSTEMS, INC
1	SCIENCE APPLICATIONS, INC 1 Von Kerczek
1	GEORGE G. SHARP
1	SPERRY SYS MGMT Lib/Shapiro
1	SUN SHIPBLDG/Lib
1	ROBERT TAGGART
1	TETRA TECH PASADENA/Furuya
1	UA HAMILTON STANDARD/Cornell

CENTER DISTRIBUTION

Copies	Code	Name
1	0120	
1	12	
1	012.1	Nakonechny
1	15	W.B. Morgan
1	1506	Hawkins
1	1509	Powell
1	152	Lin
1	1521	Day
1	1521	Karafiath
1	1521	Hurwitz
1	1522	Dobay
1	1522	Remmers
1	1522	Wilson
1	154	McCarthy
1	154.1	Yim
1	1542	Huang
1	1542	Shen
1	1542	Chang
1	1543	Platzer
1	1543	Santore
1	1544	Peterson
1	1544	Boswell
1	1544	Caster
1	1544	Reed
1	1544	Fuhs
1	1544	Jessup
20	1544	Kim
1	1544	Lin
1	156	Cieslowski
1	1561	Cox
1	1562	Davis
1	1563	Milne
1	1564	Feldman
1	172	Krenzke
1	1720.6	Rockwell
1	19	Sevik
1	1901	Strasberg
1	1905	Blake
1	1942	Archibald
1	1942	Mathews
1	1962	Zaloumis
1	1962	Noonan
1	1962	Kilcullen
1	2814	Czyryca
10	5211.1	Reports Distribution
1	522.1	TIC (C) & 1(m)
1	522.2	TIC (A)

END

FILMED

4-85

DTIC